

Dipolaritons in Quantum Dots

JUAN SEBASTIÁN ROJAS ARIAS

TESIS DE MAESTRÍA
PRESENTADA A LA FACULTAD DE CIENCIAS
DE LA UNIVERSIDAD NACIONAL DE COLOMBIA
PARA OPTAR POR EL TÍTULO DE
MAGÍSTER EN CIENCIAS - FÍSICA

DIRECTOR: DR. HERBERT VINCK POSADA

NOVIEMBRE 2015

Abstract

Dipolaritons are quasiparticles that arise in coupled quantum wells embedded in a microcavity, they are a superposition of a photon, a direct exciton and an indirect exciton. An interesting feature of dipolaritons is that their excitons can carry an electric dipole moment. Previous works have found this kind of system suitable for terahertz lasing (Phys. Rev. A 89, 023836) and Bose-Einstein condensation (Phys. Rev. B 90, 125314). In this thesis we study a system that consists of two interacting quantum dots embedded in a microcavity, from the point of view of dipolaritons in direct analogy with the quantum well case. A constant magnetic field is also taken into account.

First, the zero temperature case is studied with an exact diagonalization of a finite system hamiltonian in order to find the effects of the magnetic field on the properties of direct and indirect excitons, including their statistics. Then we include light and investigate the properties of a single dipolariton. Next, a variational approach is used to study the many-body problem and we find the effects of the magnetic field on the ground state energy and number of photons. Finally, we consider the problem at finite temperatures and use a self-consistent procedure in a Hartree-Fock-Bogoliubov approximation to find the effect of the magnetic field on the critical temperature for Bose-Einstein condensation.

Resumen

Los dipolaritones son cuasipartículas que surgen en pozos cuánticos acoplados embebidos en una microcavidad; son una superposición de un fotón, un excitón directo y un excitón indirecto. Una característica interesante de los dipolaritones es que sus excitones pueden tener un momento de dipolo eléctrico. Trabajos anteriores han encontrado este tipo de sistemas como candidatos para emisión en terahertz (Phys. Rev. A 89, 023836) y condensación de Bose-Einstein (Phys. Rev. B 90, 125314). En esta tesis se estudia un sistema compuesto de dos puntos cuánticos interactuantes embebidos en una microcavidad, desde el punto de vista de los dipolaritones en analogía directa con el caso de pozos cuánticos. Se incluye, además, un campo magnético constante.

Primero, el caso a temperatura cero se estudia con la diagonalización exacta de un hamiltoniano de sistemas finitos, con el objetivo de encontrar los efectos del campo magnético en las propiedades de excitones directos e indirectos, incluyendo su estadística. Luego se incluye la luz y se investigan las propiedades individuales de un dipolariton. Posteriormente, un tratamiento variacional se desarrolla para estudiar el problema de muchos cuerpos y encontrar los efectos del campo magnético en la energía del estado base y el número de fotones. Finalmente, se considera el problema a temperatura finita y se utiliza un procedimiento autoconsistente en la aproximación de Hartree-Fock-Bogoliubov para encontrar el efecto del campo magnético en la temperatura crítica para la condensación de Bose-Einstein.

Agradecimientos

Agradezco especialmente a mi papá, mi mamá y mi hermano, puesto que ellos han sido la compañía y el apoyo constante a lo largo de toda mi vida. Todo esfuerzo y paso hacia el progreso es gracias y en honor a ellos.

Al profe Herbert, quien me introdujo al mundo de la investigación y me ha motivado a explotar mis capacidades al máximo. El 90% de la física de este trabajo la aprendí de él.

A Cata, quien me ha complementado y soportado durante varios años.

A Rulos, que lo conocí en mis primeros días de universidad y se ha convertido en el mejor amigo que pude tener.

A Lorena, Josele, Rafa y Ángela, con quienes he pasado muy buenos momentos y siempre me han hecho valorar lo que hago.

A los compañeros del grupo de investigación, que son demasiados para mencionar uno por uno, ha sido maravilloso discutir con ellos la física y compartir una amistad.

Al Dr. Dario Gerace de la Università di Pavia, con quien fue posible discutir este trabajo gracias al apoyo financiero por parte de Colciencias, en el proyecto de código 110156933525, contrato número 026-2013 y código HERMES 17432.

Para mis padres...

Publications and Conferences

Results obtained from this work have been presented as posters at the following conferences:

- *Quantum Optics VII* , Mar del Plata - Argentina.
- *Gordon Research Conferences: Quantum control of light and matter*, South Hadley - USA.

During the development of this thesis the following conference proceeding was written and published:

- J. S. Rojas-Arias, L. A. Briceño-Villalba, and H. Vinck-Posada, "*Finite System Theory of Two Interacting Quantum Dots in an Optical Microcavity*", in *Advanced Photonics 2015*, OSA Technical Digest (online) (Optical Society of America, 2015), paper JM3A.20.

From this thesis two articles were written and are pendant for publication:

- J. S. Rojas-Arias, B. A. Rodríguez, H. Vinck-Posada, "*Magnetic control of dipolaritons in quantum dots*".
- J. S. Rojas-Arias, B. A. Rodríguez, H. Vinck-Posada, "*Bose-Einstein condensation of dipolaritons in quantum dots*".

Contents

Abstract	iii
Resumen	v
Agradecimientos	vii
Publications and Conferences	xi
List of Figures	xv
1 Introduction	1
1.1 Semiconductor heterostructures	2
1.1.1 Microcavities	3
1.1.2 Quantum wells and dots	3
1.2 Quasiparticles	5
1.2.1 Excitons	6
1.2.2 Polaritons	7
1.3 Dipolaritons	8
1.4 State of the art	10
1.4.1 Cristofolini et al. (2012)	10
1.4.2 Kyriienko et al. (2014)	11
1.4.3 Shelykh et al. (2013-2014)	12
1.4.4 Byrnes et al. (2014)	13
2 Physical System and Model	15
2.1 Effective mass approximation	15
2.2 Confining potential in a QD	16
2.3 Charge carriers in a QD	18
2.3.1 $B = 0$	19
2.3.2 $B \neq 0$	20

2.4	Light-matter interaction	21
2.5	Physical system and Hamiltonian	22
3	Excitons in QDMs: Properties of Direct and Indirect Excitons	27
3.1	Theory	27
3.2	Effects of magnetic field on a single exciton	29
3.3	Statistics of exciton operators	31
4	Dipolaritons in QDs: Exact Diagonalization	37
4.1	Theory	38
4.2	Dipolariton modes	38
4.3	Effects of magnetic field on a single dipolariton	40
4.4	Emission	41
5	Multiexcitonic QDs: Zero Temperature Variational Method	45
5.1	Theory	45
5.2	Effects of magnetic field on multiexcitonic QDMs	47
5.3	Statistics of exciton operators	49
6	Bose-Einstein Condensation of Dipolaritons: Finite Temperature Variational Method	53
6.1	Theory	54
6.2	Bose-Einstein condensation of dipolaritons	58
7	Conclusions	61
7.1	Future Work	62
A	Coulomb Matrix Elements	63
A.1	Solving the integral	64
A.2	Series acceleration	67
	Bibliography	69

List of Figures

1.1	Scanning Electron Micrograph of a microcavity	3
1.2	Schematic picture of a quantum well, wire and dot	4
1.3	SEM image of a sample of InAs quantum dots grown on GaAs	4
1.4	Two masses held together by a spring	5
1.5	Scheme of an electron that “jumps” from the valence band to the conduction band	7
1.6	Scheme of two coupled QWs	9
1.7	Energy and composition of the dipolariton branches	11
1.8	Second order correlation function for different values of the detunings	12
1.9	Ratio of various contributions in the total dipolariton interaction energy as a function of the interwell distance	13
2.1	Band structure of InGaAs	16
2.2	Cross-section TEM of an InAs QD grown on GaAs	17
2.3	Physical system	23
3.1	Energy of the IX and DX as a function of the magnetic field	30
3.2	Energy and composition of the ground and first excited state, as a function of the magnetic field, for the system without light	31
3.3	Mean value of the exciton operators’ commutator as a function of the Coulomb interaction strength	34
4.1	Energy and composition of the dipolariton branches in QDs	39
4.2	Energy and composition of the ground and first excited state, as a function of the magnetic field, for the system with light	41
4.3	Energy position and intensity of the emission line as a function of the number of dipolaritons	42

5.1	Number of photons vs the magnetic field and dipolariton number	48
5.2	Scaling of the total energy as a function of the magnetic field	48
5.3	Mean value of the variational exciton operators' commutator as a function of the Coulomb interaction strength	50
6.1	Temperature dependence of the number of photons in the condensate and the chemical potential	58
6.2	Scaling of the critical temperature	59
A.1	Scheme of two charge carriers in different layers	63

Chapter 1

Introduction

One of the most interesting and important problems in physics corresponds to the many-body one. It is well known in classical mechanics that even the problem of 3 particles interacting via a gravitational potential has not an exact general solution; in quantum mechanics the situation isn't so different although there are techniques such as the Faddeev equations which allow to solve the non-perturbative problem iteratively [15]. However, when the number of particles is greater than 3 the exact system becomes unsolvable. Several approximations are used in order to deal with this, such as perturbation theory, mean field approximation and density functional theory [17]. A lot of effort has been made to find new techniques for the treatment of the many-body problem since its applications range from condensed matter physics to quantum chromodynamics. One of the principal techniques used to deal with the many-body problem is the picture of quasiparticles which is the one we will focus in this work [34].

On the other hand, the improvement of experimental techniques on semiconductor materials has allowed the development of methods to study the properties and phenomena present in finite systems of electrons and photons [40], and in turn, the creation and control of quasiparticles such as excitons and polaritons. Semiconductor structures such as Quantum Wells (QWs), Quantum Wires and Quantum Dots (QDs), which restrict the movement of charge carriers to two, one and zero dimensions, respectively, are of great research interest due to their potential technological applications in quantum computation and high-efficiency optoelectronics. Furthermore, the introduction of these structures in microcavities, allowing

the interaction with light, has enabled the Bose-Einstein condensation in solid-state systems [4].

This chapter presents the background that justifies the motivation of the work and gives the necessary tools for its understanding. First, we present the systems of interest and mention some experimental aspects. Then, we give an overview of the concept of quasiparticle and introduce *excitons* and *polaritons* which are essential quasiparticles for the description of our system. With this, we present the quasiparticle of main interest in the work: *dipolariton*. Finally, we conclude with a review on the state of the art of dipolariton-related research.

1.1 Semiconductor heterostructures

The Purcell effect consists of the placing of an optical emitter inside a cavity in order to tune its relaxation time. This effect had been first looked for atoms in cavities but with the goal of a massive technological implementation the solid state also started pursuing this effect. The typical examples are quantum dots (QDs) or quantum wells (QWs) placed in cavities made in micropillars, microdisks, or photonic crystals [31].

Several advantages can be found in semiconductor systems in comparison with other candidate systems for quantum computation. The first one to be mentioned is their size, which lies on the range of nanometres to micrometres while, for example, atomic systems have typical sizes of the order of centimetres. Other advantages to be mentioned are their ease to connect with electronics and the control of their shape and interactions with state-of-the-art nanostructure fabrication techniques. However, there is a common disadvantage in almost all solid state devices: dissipation. Semiconductor systems will always be affected by the huge amount of interactions with the rest of the crystalline media. The presence of other particles and lattice vibrations due to temperature introduces decoherence to the system and an eventual break-up of the quantum behaviour. Despite this, the improvement on the fabrication techniques and experimental conditions keep semiconductor devices as strong candidates for future electronics.

1.1.1 Microcavities

A microcavity is an optical resonator close to, or below the dimension of the wavelength of light [26]. We will focus on microstructures periodically patterned on the scale of the resonant optical wavelength (Fig. 1.1). This kind of structures use interference in order to confine light in a defect.

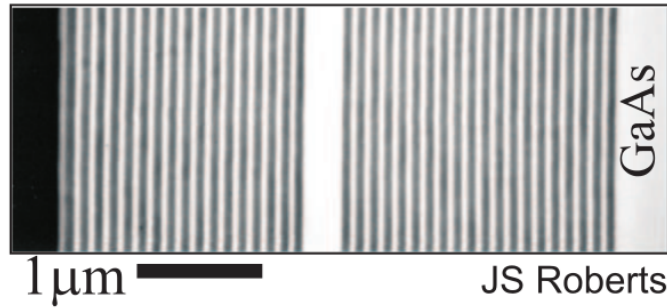


Figure 1.1: Scanning Electron Micrograph (SEM) of a GaAs/AlGaAs DBR microcavity on a GaAs substrate. Image taken from Ref. [26].

The periodic layers have a width such that reflected light satisfies a condition of constructive interference and transmitted light a condition of destructive interference, this structure is known as *Distributed Bragg Reflector* (DBR). This condition can only be achieved for a specific wavelength so that this kind of microcavities work for a specific light frequency.

A defect, consisting of a thicker layer of a material, is introduced, this defect is the microcavity and the periodic layers surrounding it work as mirrors that keep light confined. The mirrors' reflectance depends on the materials, the number of layers and the quality of the fabrication i.e., amount of impurities, layers' width, parallelism, etc.

1.1.2 Quantum wells and dots

A quantum well (QW) is a structure that confines the movement of charge carriers in one dimension, so the carriers are free particles in the other two dimensions, for this reason the QWs are known as 2D systems. Similarly, quantum wires and dots are defined by the number of dimensions in which the charge carriers can move freely, as shown in Fig. 1.2. QWs have quantisation in only one direction, in contrast, QDs are fully quantised systems (artificial atoms).

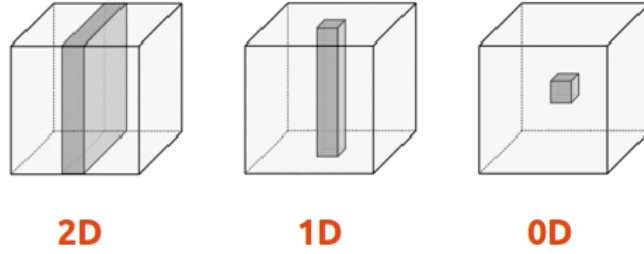


Figure 1.2: Schematic picture of a quantum well (2D), wire (1D) and dot (0D). Image edited from Ref. [37].

In semiconductor materials, the fabrication of quantum dots by physical methods can be done by Stranski-Krastanow growth [38] in which alternating layers of two materials with similar lattice constants are deposited over a substrate, in this way, a periodic structure (DBR) is produced. Then, a layer of a material with a different lattice constant is deposited. This difference in the lattice constant generates strains on the layer that will eventually relax to a lower energy state, with the formation of randomly positioned “islands”, passing from a 2D to a 3D structure as can be seen in Fig. 1.3. These “islands” are the QDs. When fabricated by this procedure are known as *self-assembled quantum dots*, nevertheless, they can also be fabricated with state-of-the-art lithography techniques to have control over their position and shape. The layer on which the QDs are located is known as *wetting layer* and may be of great impact on QDs’ dynamics [3].

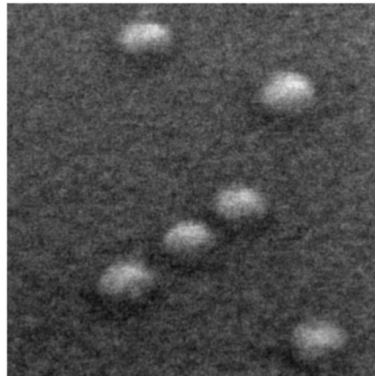


Figure 1.3: SEM image of a sample of InAs quantum dots grown on GaAs. The field of view is $150 \times 150 \text{ nm}^2$. Image taken from Ref. [38].

These structures are made of semiconductor materials, which means that there is a gap between the valence and conduction bands. If sufficient energy is given to the medium,

an electron from the valence band may “jump” to the conduction band [23]. One way to provide the necessary energy for this to happen is to place one of the structures illustrated in Fig. 1.2 inside a microcavity (Fig. 1.1), such that confined photons in the cavity are eventually absorbed by the structure, generating a matter excitation. In this way, a QW, for example, will act as the optical emitter placed in a cavity for the Purcell effect.

We are interested on the placing of QWs and QDs inside a microcavity. In this situation, the complex interactions between matter and light-matter, require the use of specialized theoretical methods for its description. Next section will approach this topic.

1.2 Quasiparticles

As mentioned above, the quasiparticle formulation of the many-body problem is one of the most used and successful. It replaces the real problem with an effective one. A really good explanation of what quasiparticles are is presented in Ref. [34], here we will only present a summary.

The motion of several interacting particles is impossible to describe if the interactions are not perturbative. However, a new simple picture of matter emerges from the quantum field theory, in which systems of interacting real particles are described in terms of approximately non-interacting fictitious bodies called “quasiparticles”.

Let us consider a simple example on how this can happen. Suppose a system of two masses (m_1 and m_2) which are attached by a spring as is shown in Fig. 1.4. The system is also under the action of a gravitational field. The motion of each body separately is really complicated to describe because of the interaction between the two bodies via the spring.

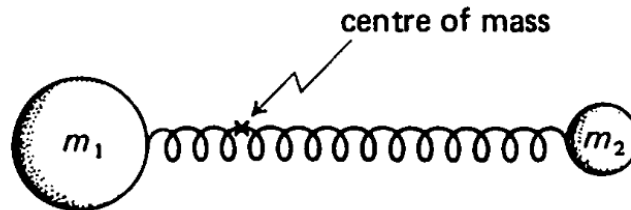


Figure 1.4: Two masses held together by a spring. Image taken from Ref. [34].

“However, we can break up the complicated motion into two independent simple motions: motion of the centre of mass and motion about the centre of mass. The centre of mass moves exactly as if it were an independent body of mass $m_1 + m_2$, so it is one of the non-interacting fictitious bodies here. The other fictitious body is a body of mass $m_1 m_2 / (m_1 + m_2)$ -the so-called ‘reduced mass’-which moves independently relative to the centre of mass. Thus the system acts as if it were composed of two non-interacting fictitious bodies: the ‘centre of mass body’ and the ‘reduced mass body’.” [34]

This simple classical example illustrates pretty well the idea of quasiparticles. The following sections will be to present the quasiparticles involved in the work.

1.2.1 Excitons

Excitations of matter consist of an electron that acquires sufficient energy to go from the Valence Band (VB) to the Conduction Band (CB). The VB gains a net positive charge known as *hole* (Fig. 1.5). This hole is a quasiparticle used to describe the absence of charge in the valence band, so it will have the electron charge but with opposite sign; an effective mass is associated to the hole too. There are two kinds of holes: *light holes* and *heavy holes*, with the latter being the ones with the most important effects in common systems [23, 24].

The electron in the CB interacts with the hole via Coulomb interaction. This interaction may generate a bound state of an electron and a hole, similar to the one generated by the two masses interacting via a spring in the previous example, and is known as an *exciton*. Excitons are another kind of quasiparticles and are common to describe the excitations of matter [23]. They have no charge and since they are composed of two fermions, excitons are basically bosons. It can be shown that exciton creation b_q^\dagger and annihilation b_q operators follow bosonic commutation rules at low densities [32, 12, 11], this is:

$$[b_q, b_{q'}^\dagger] \approx \delta_{q,q'}, \quad (1.1)$$

however, at high densities the fermionic nature of the particles excitons are composed of, becomes relevant and the commutation rule (1.1) requires corrections.

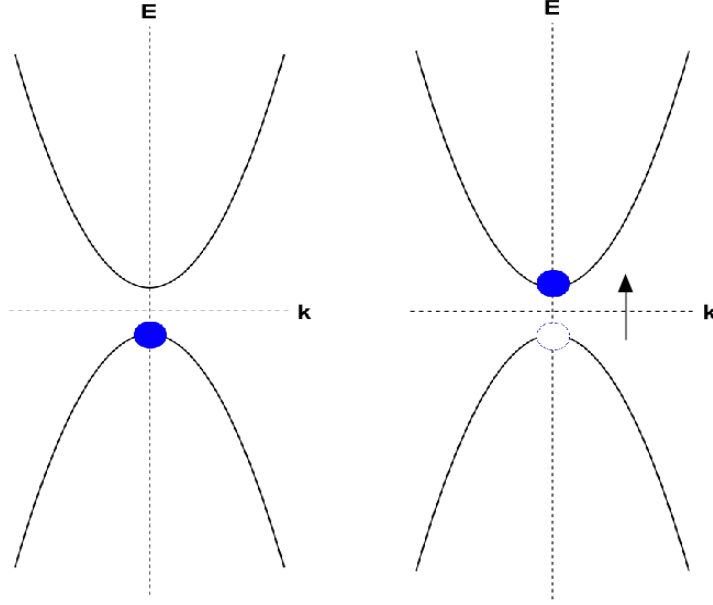


Figure 1.5: Scheme of an electron (blue) that “jumps” from the valence band to the conduction band, leaving a “hole” (white) with a net positive charge.

1.2.2 Polaritons

As was mentioned before, one way to generate the jump of an electron to the conduction band is by the absorption of a photon, so, the light might generate those electron-hole pairs known as excitons. The second quantization hamiltonian that describes this situation in a QW is as follows [23]:

$$H = \sum_q [\hbar e_q b_q^\dagger b_q + \hbar \omega_q a_q^\dagger a_q + (\hbar g_q b_q^\dagger a_q + \text{h.c.})], \quad (1.2)$$

with a_q (a_q^\dagger) the annihilation (creation) operator of photons in the cavity, $\hbar e_q$ and $\hbar \omega_q$ the energies of excitons and photons, and $\hbar g_q$ the strength of the light matter interaction. The Hamiltonian from Eq. 1.2 has two approximations known as *dipolar approximation* and *rotating wave approximation* [19]; in the first one, the amplitude of the electric field is considered constant along the optical emitter’s volume; in the second one, non-rotating terms ($b_q^\dagger a_q^\dagger$ or $b_q a_q$) can be neglected in the near-resonance situation ($\hbar \omega_q \sim \hbar e_q$).

We now define the *polariton operators* p_q^{LP} and p_q^{UP} as a linear combination of exciton and photon operators:

$$\begin{aligned}
p_q^{UP} &= u_q b_q - v_q a_q, \\
p_q^{LP} &= v_q^* b_q + u_q^* a_q,
\end{aligned}
\tag{1.3}$$

and demand polariton operators to obey Bose commutation rules:

$$[p_q^{UP}, p_q^{UP\dagger}] = |u_q|^2 + |v_q|^2 = 1, \tag{1.4}$$

and similarly for p_q^{LP} . The coefficients are chosen such that the hamiltonian becomes diagonal [23], obtaining:

$$H = \sum_q (\hbar\Omega_q^{LP} p_q^{LP\dagger} p_q^{LP} + \hbar\Omega_q^{UP} p_q^{UP\dagger} p_q^{UP}), \tag{1.5}$$

with [31]:

$$\Omega_q^{LP,UP} = \frac{1}{2}(e_q + \omega_q) \pm \frac{1}{2}\sqrt{(e_q - \omega_q)^2 + 4g_q^2}. \tag{1.6}$$

We see that the hamiltonian of interacting excitons and photons (Eq. 1.2) can be written as a hamiltonian of non interacting quasiparticles called *polaritons* (Eq. 1.5). From Eq. 1.6 we see that there are two polariton branches known as *upper polariton* (+, UP) and *lower polariton* (-, LP).

The Bogoliubov transformation (1.3) can only be performed at the low density limit, in which Eq. (1.1) is valid. In this limit, polariton operators follow Bose commutation rules and are able to condensate [4].

1.3 Dipolaritons

Dipolaritons have a great analogy with polaritons, in fact, they are polaritons with a large dipole moment. They appear in a system of coupled QWs as the one presented in Fig. 1.6 where two QWs are embedded in an optical microcavity and separated by a distance d . The QWs are coupled via electron tunnelling allowing the formation of an electron-hole

bound state with the particles in different layers known as *indirect exciton* (IX); the usual exciton with the charges in the same layer will be called *direct exciton* (DX) [22].

Excitons are quasiparticles with a probability of recombination, thus, they have a lifetime. This probability depends on the overlapping of the electron and hole wave functions [21, 22]. Direct excitons have a lifetime of less than 100ps [20], while indirect excitons, in which the spatial separation of the QWs decreases the wave functions' overlapping, can reach tens or hundreds of microseconds [7, 8, 18]. For this reason we expect dipolaritons to have a longer lifetime than polaritons.

The photons C in the cavity interact with the DX and the latter is coupled with the IX via tunnelling. The photonic modes do not couple with the IX modes. A bias voltage is applied in order to inhibit hole tunnelling (green arrow in Fig. 1.6) [13].

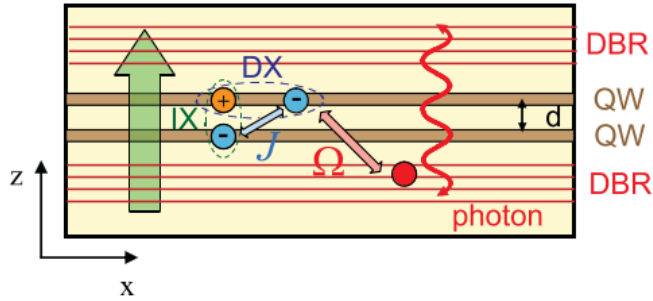


Figure 1.6: Scheme of two coupled QWs. The QWs are coupled via tunnelling J , one QW interacts with light Ω . Image taken from Ref. [10].

The hamiltonian is pretty similar to the one in Eq. 1.2 but adding the possible tunnelling $\hbar J$ between direct and indirect excitons [10], in a matrix form can be written as:

$$H = \begin{pmatrix} \frac{\hbar^2 q^2}{2m_{ph}} + \delta_{ph} & \hbar g & 0 \\ \hbar g & \frac{\hbar^2 q^2}{2M} & \hbar J \\ 0 & \hbar J & \frac{\hbar^2 q^2}{2M} + \delta_{IX} \end{pmatrix}, \quad (1.7)$$

where m_{ph} is the effective mass of the photons, M the one for the excitons, and δ_i are possible detunings between the energies. By using a similar procedure to the one used in the preceding section, the hamiltonian Eq. 1.7 can be diagonalized as:

$$H = \sum_q [\varepsilon_q^{LP} p_q^{LP\dagger} p_q^{LP} + \varepsilon_q^{MP} p_q^{MP\dagger} p_q^{MP} + \varepsilon_q^{UP} p_q^{UP\dagger} p_q^{UP}], \quad (1.8)$$

where $\varepsilon_q^{LP,MP,UP}$ are the eigenvalues of Eq. 1.7. Here we can distinguish that in contrast with the previous case, we have three polariton branches with MP being the *middle polariton* branch [13].

Dipolaritons are, then, quasiparticles formed by a three way superposition of a direct exciton DX, an indirect exciton IX and a cavity photon C. They are also bosons but differ from polaritons in the fact that their IX component provides them with an electric dipole moment, due to the separation between wells, and a longer lifetime.

Dipolaritons are the quasiparticles of main interest in this thesis since they have very interesting properties, mentioned in the following section, that might allow the development of several optoelectronic devices of great interest for quantum computation.

These quasiparticles are proposed in quantum wells, the main question to answer in this text is: **What about dipolaritons in Quantum Dots?**

1.4 State of the art

In this section we present a summary of some interesting articles related with dipolaritons, that motivated this thesis, and illustrate the state of the art in dipolariton-related research.

1.4.1 Cristofolini et al. (2012)

In this work (Ref. [13]), the authors use Molecular Beam Epitaxy (MBE) to grow a $\frac{5}{2}\lambda$ cavity, designed to work for $\lambda = 880\text{nm}$, with 21 and 17 periods of GaAs/AlAs as distributed Bragg reflectors. Four sets of asymmetric double quantum wells (ADQWs), 10nm wide, are inside the microcavity, positioned at the antinodes of the optical field. They use three samples in which the QWs are separated by barriers with widths of 4nm, 7nm and 20nm, so they can access different tunnelling coupling strengths. A bias voltage can be applied across the microcavity through electric contacts.

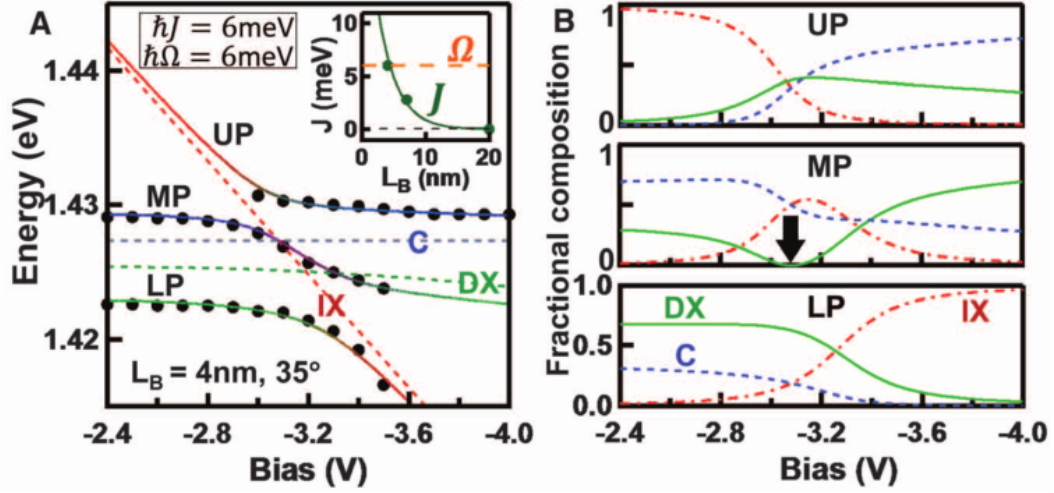


Figure 1.7: (A) Bias-dependent dipolariton modes observed in photoluminescence for a barrier width of 4nm (dots) and fits to an effective model (solid lines). Dashed lines mark bare energies. Inset: Extracted intrinsic tunnelling rate J as a function of the barrier width (points) together with theory (line). (B) Bias dependence of the dipolariton composition. Image taken from Ref. [13].

The authors perform optical measurements in a liquid helium cryostat ($T \sim 10$ K). Each mesa is excited non-resonantly by a Ti-sapphire laser (CW 800nm) with $200 \mu\text{W}$ focussed to a $100 \mu\text{m}$ diameter spot. Among several results, Fig. 1.7 is obtained, there, the bias voltage is used to vary IX's energy and the three dipolariton branches are found. They use an effective model to fit the experimental results and determine the composition of each branch.

1.4.2 Kyriienko et al. (2014)

In this paper (Ref. [30]), the authors study theoretically the system of two QWs in a microcavity. The hamiltonian used is:

$$\begin{aligned}
 H = & \hbar\omega_C a^\dagger a + \hbar\omega_{DX} b^\dagger b + \hbar\omega_{IX} c^\dagger c + \frac{\hbar\Omega}{2} (a^\dagger b + b^\dagger a) - \frac{\hbar J}{2} (b^\dagger c + c^\dagger b) \\
 & + P e^{-i\omega_p t} a^\dagger + P^* e^{i\omega_p t} a + V_{dd} b^\dagger b^\dagger b b + V_{ii} c^\dagger c^\dagger c c + V_{di} b^\dagger c^\dagger b c,
 \end{aligned} \tag{1.9}$$

where $\hbar\omega_C$, $\hbar\omega_{DX}$ and $\hbar\omega_{IX}$ denote the cavity mode, direct exciton, and indirect exciton energies, respectively. $\hbar\Omega$ denotes the Rabi-splitting and $\hbar J$ the tunnelling. A coherent

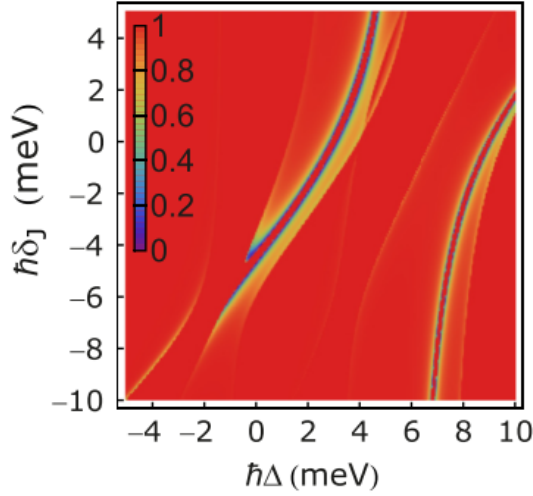


Figure 1.8: Second order correlation function for different values of the detunings. Image taken from Ref. [30].

optical pumping of the cavity mode with rate P and frequency ω_p is taken into account. V_{dd} , V_{ii} and V_{di} are the nonlinear many-body interactions between excitons. A master equation with dissipative terms written in a Lindblad form is solved in order to calculate the mean number of photons and the second order correlation function.

Fig. 1.8 shows the dependence of the second order correlation function with the detunings defined as: $\Delta = \omega_p - \omega_C$ and $\delta_J = \omega_{IX} - \omega_{DX}$. There are zones in which the correlation function is almost zero, in these regimes the emission is antibunched and the system is suitable for single-photon emission. It is important to notice that both detunings can be controlled: Δ with the frequency of the pumping and δ_J with an electric field.

1.4.3 Shelykh et al. (2013-2014)

This research (Refs. [27, 28, 29]) uses effective models similar to that used in the previous subsection. The authors consider the two coupled QWs to be embedded in a terahertz (THz) microcavity and calculate the dynamics of the excitons' populations. One of the main findings consists of the IX population oscillating with THz frequency. Since the IX composition provides the overall electric dipole moment of the system, this situation corresponds to a time-varying dipole that should emit continuous wave (CW) radiation in

the THz range. Furthermore, the frequency of the emission can be tuned by means of an electric field, and has output powers that may compete with current THz sources.

1.4.4 Byrnes et al. (2014)

In this work (Ref. [10]), the bosonic statistics of dipolaritons are exploited and used to determine the possibility of a dipolariton condensate. To do this, the authors exhaustively investigate the effective interactions between excitons. Fig. 1.9 shows the ratio of various contributions in the total dipolariton interaction energy as a function of the interwell distance. There it can be seen that the most relevant interactions are between excitons of the same type and that the interaction between IXs is of the same order than that between DXs.

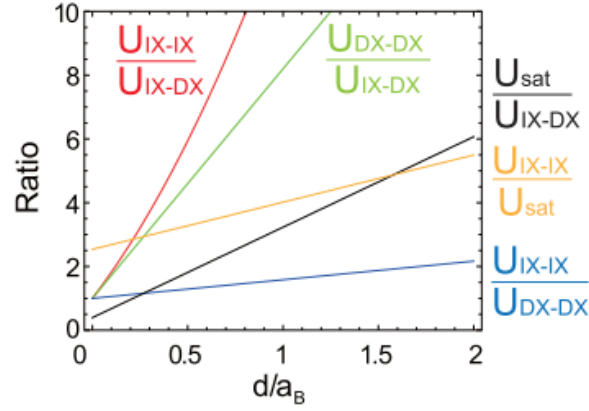


Figure 1.9: Ratio of various contributions in the total dipolariton interaction energy as a function of the interwell distance d . Image taken from Ref. [10].

In the same paper the authors conclude that dipolaritons may be able to Bose-Einstein condensate and using a dissipative Gross-Pitaevskii are able to determine that parameters for condensation of dipolaritons are pretty similar to those of polaritons.

Chapter 2

Physical System and Model

Quantum dots, as fully quantised systems, present interesting phenomena not present in QWs. Quantum mechanics appears at its maximum expression due to the small number of excitons that QDs usually confine in contrast with QWs where a large number of excitons is created when the system is excited.

Several models can be used to describe quantum dots, the most popular one might be the Jaynes-Cummings effective hamiltonian in which the QD is approximated as a two-level system [19]. We will use a more precise one that starts from the basics: electrons confined in a structure.

This chapter is dedicated to the introduction of the physical system to be modelled in the rest of the text and the derivation of the corresponding hamiltonian.

2.1 Effective mass approximation

In order to model a QD it is necessary to look first at the band structure of the material it is made of. We consider quantum dots made of InGaAs. Figure 2.1 displays the band structure of InGaAs, there, we see that for $k \approx 0$, the bands can be approximated as parabolas, which allows us to write:

$$E(k) \approx E_{gap} + \frac{\hbar^2 k^2}{2m^*}, \quad (2.1)$$

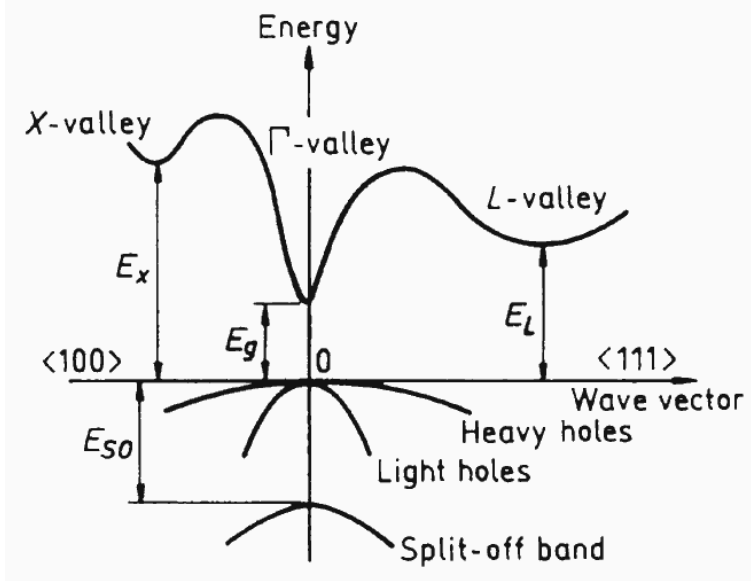


Figure 2.1: Band structure of InGaAs. We are considering the region close near the Γ -valley. Image taken from Ref. [1].

where E_{gap} represents the band gap of the semiconductor material and the quantity m^* is the *effective mass* of the electrons [23] that plays an important role: knowing the effective mass in the semiconductor, the problem of a particle inside the material can be reduced in an effective way, to a free particle with mass m^* . Electrons in the Valence Band (VB) will have a negative effective mass, but in order to avoid dealing with negative masses, it is often preferred to introduce holes as new quasi-particles with a positive mass and positive charge. Then, we will refer to electrons in the conduction band just as electrons, and the absent charges in the valence band will be the holes.

In Fig. 2.1 we see that for the valence band there are two levels labelled as *Heavy holes* and *Light holes*, in our treatment we will consider heavy holes only because they have a stronger coupling with light than light holes [5, 48].

2.2 Confining potential in a QD

Charge carriers will be confined in a QD, for this reason it is important to have a model of the confining potential the particles feel in it. In this section we will follow the theory from Ref. [38] to show that the particles in a QD are subject to a 2D harmonic potential.

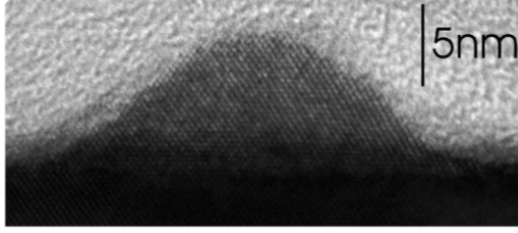


Figure 2.2: Cross-section TEM of an InAs QD grown on GaAs. Image taken from Ref. [38].

Although the reference focus its attention on self-assembled QDs, the harmonic potential is usually used to model other kinds of quantum dots.

We start with a single electron in a QD, subject to a confining potential $V(r, z)$, then we write the Schrödinger equation in cylindrical coordinates:

$$\left[\frac{-\hbar^2}{2m_e} \left[\frac{1}{r^2} \left(r \frac{\partial}{\partial r} r \frac{\partial}{\partial r} + \frac{\partial^2}{\partial \theta^2} \right) + \frac{\partial^2}{\partial z^2} \right] + V(r, z) \right] \Psi(r, \theta, z) = E \Psi(r, \theta, z), \quad (2.2)$$

where m_e is the effective mass of the electron in the material. Due to the low aspect ratio of self-assembled quantum dots (see Fig. 2.2), the confinement in the growth direction (z axis) dominates, and only one bound state exists for motion in this direction; the motion in the plane can be considered separately [51]. Therefore, the wavefunction can be expressed as the product: $\Psi(r, \theta, z) = Z(z)f(r, \theta)$. Replacing this result in the Schrödinger equation and separating variables we get the following two equations:

$$\left[\frac{-\hbar^2}{2m_e} \frac{1}{r^2} \left(r \frac{\partial}{\partial r} r \frac{\partial}{\partial r} + \frac{\partial^2}{\partial \theta^2} \right) + E_0(r) \right] f(r, \theta) = E f(r, \theta) \quad (2.3)$$

$$\left[\frac{-\hbar^2}{2m_e} \frac{\partial^2}{\partial z^2} + V(r, z) \right] Z(z) = E_0(r) Z(z) \quad (2.4)$$

Now, we need a model for the potential $V(r, z)$; this model should depend on the shape of the dot. Along the z direction we consider the potential to be zero inside the dot and to have a finite value V_0 outside, thus, we will have a finite well with a width that depends on the radial position r . The energy levels of the finite well can be written, at first order correction, in terms of the solution to the infinite well as:

$$E_{\text{finite}}(r) \approx \frac{P^2}{1 + P^2} E_{\text{infinite}}(r) = \frac{P^2}{1 + P^2} \frac{\hbar^2 \pi^2}{2m_e t(r)^2}, \quad (2.5)$$

where $P = L_0 \sqrt{2m_e V_0} / 2\hbar$, $t(r)$ is the thickness of the well for each radial position, and $L_0 = t(0)$ is the dot's height. What is left now is to determine the shape of the dot, i.e., the function $t(r)$. Fig. 2.2 displays a Transmission Electron Microscopy of a self-assembled QD, there it can be seen that the dot has a paraboloid-like shape, such that $t(r)$ is given by:

$$t(r) = L_0 \left(1 - \frac{r^2}{r_0^2} \right), \quad (2.6)$$

with r_0 the greater radius of the dot. Introducing this expression in Eq. (2.5) and performing binomial expansion in r , keeping only the terms up to order 2, we obtain:

$$E_0(r) = \frac{P^2}{1 + P^2} \frac{\hbar^2 \pi^2}{2m_e L_0} \left[1 + 2 \left(\frac{r}{r_0} \right)^2 \right] := \frac{1}{2} m_e \omega_0^2 r^2 + E_0^e. \quad (2.7)$$

Finally, replacing Eq. (2.7) in Eq. (2.3) we see that in the plane the particle is subject to an offset harmonic oscillator potential. The offset energy E_0^e corresponds to Eq. (2.7) evaluated at $r = 0$.

We note that the shape of the QD determines the strength of the parabolic confinement in an inverse way; the smaller the dot, the stronger the confinement ω_0 . Also, the effective mass affects the confinement, so, in general, electrons and holes will be subject to a different strength of the confinement.

Knowing the confining potential, in the following sections we will present the derivation of the hamiltonian for several charge carriers in a QD and the light-matter interaction.

2.3 Charge carriers in a QD

We now consider a set of N electrons and holes confined in a QD and interacting through Coulomb potential. The particles will be subject to a parabolic confinement [38] and

a magnetic field B will be applied in the z direction. With this considerations, the hamiltonian of charge carries in the QD can be written as:

$$\begin{aligned}
H = & \sum_{i=1}^N \frac{1}{2m_e} \left(\vec{P}_{e_i} + \frac{e}{c} \vec{A}_{e_i} \right)^2 + \sum_{i=1}^N \frac{1}{2} m_e \omega_e^2 r_{e_i}^2 + \frac{e^2}{\varepsilon} \sum_{i < j} \frac{1}{|\vec{r}_{e_i} - \vec{r}_{e_j}|} \\
& + \sum_{j=1}^N \frac{1}{2m_h} \left(\vec{P}_{h_j} - \frac{e}{c} \vec{A}_{h_j} \right)^2 + \sum_{j=1}^N \frac{1}{2} m_h \omega_h^2 r_{h_j}^2 + \frac{e^2}{\varepsilon} \sum_{i < j} \frac{1}{|\vec{r}_{h_i} - \vec{r}_{h_j}|} \\
& - \frac{e^2}{\varepsilon} \sum_{i,j} \frac{1}{|\vec{r}_{e_i} - \vec{r}_{h_j}|},
\end{aligned} \tag{2.8}$$

where $m_{e(h)}$ is the effective mass of electrons (holes), $\vec{r}_{e_i(h_j)}$ and $\vec{P}_{e_i(h_j)}$ are the bi-dimensional position and momentum vectors for electrons (holes) and $\hbar\omega_{e(h)}$ are the energies associated with the parabolic confinement. ε is the permittivity of the material, InGaAs in this case. \vec{A} is the vector potential associated to the magnetic field. We will ignore spin degrees of freedom, for this reason, Zeeman splitting terms do not appear in Eq. (2.8), this can be done because Coulomb interaction does not change the spins' orientation, also, we only consider one polarization of light that will couple to one orientation of the spins.

The transition to the second quantisation formalism will depend on the situation: $B = 0$ or $B \neq 0$.

2.3.1 $B = 0$

First we turn off the magnetic field and focus on the particular case in which electrons and holes have the same effective masses and are subject to the same confinement strength: $\omega_e = \omega_h = \omega_0$ and $m_e = m_h = \mu$, then the hamiltonian (2.8) is reduced to:

$$\begin{aligned}
H = & \sum_{i=1}^N \frac{1}{2\mu} P_{e_i}^2 + \sum_{j=1}^N \frac{1}{2\mu} P_{h_j}^2 + \sum_{i=1}^N \frac{1}{2} \mu \omega_0^2 r_{e_i}^2 + \sum_{j=1}^N \frac{1}{2} \mu \omega_0^2 r_{h_j}^2 \\
& + \frac{e^2}{\varepsilon} \sum_{i < j} \frac{1}{|\vec{r}_{e_i} - \vec{r}_{e_j}|} + \frac{e^2}{\varepsilon} \sum_{i < j} \frac{1}{|\vec{r}_{h_i} - \vec{r}_{h_j}|} - \frac{e^2}{\varepsilon} \sum_{i,j} \frac{1}{|\vec{r}_{e_i} - \vec{r}_{h_j}|}.
\end{aligned} \tag{2.9}$$

Defining the oscillator length $l_O = \sqrt{\hbar/\mu\omega_0}$ we realize the transformation to dimensionless variables: $\vec{r} \rightarrow l_O\vec{r}$ and $\vec{P} \rightarrow \frac{\hbar}{l_O}\vec{P}$, obtaining:

$$H = \frac{\hbar\omega_0}{2} \sum_{i=1}^N \left(P_{e_i}^2 + P_{h_j}^2 + r_{e_i}^2 + r_{h_j}^2 \right) + \frac{e^2}{\varepsilon l_O} \left(\sum_{i<j} \frac{1}{|\vec{r}_{e_i} - \vec{r}_{e_j}|} + \sum_{i<j} \frac{1}{|\vec{r}_{h_i} - \vec{r}_{h_j}|} - \sum_{i,j} \frac{1}{|\vec{r}_{e_i} - \vec{r}_{h_j}|} \right). \quad (2.10)$$

Now, we choose the 2D harmonic oscillator states as single-particle basis and write the hamiltonian in the second quantisation formalism, with e_i ($h_{\bar{i}}$) and e_i^\dagger ($h_{\bar{i}}^\dagger$) the fermionic annihilation and creation operators of an electron (hole) in the state i , respectively:

$$\frac{H}{\hbar\omega_0} = \sum_n t_n (e_n^\dagger e_n + h_{\bar{n}}^\dagger h_{\bar{n}}) + \beta \sum_{rsuv} \langle rs|V(0)|uv\rangle e_r^\dagger e_s^\dagger e_v e_u + \beta \sum_{rsuv} \langle \bar{r}\bar{s}|V(0)|\bar{u}\bar{v}\rangle h_{\bar{r}}^\dagger h_{\bar{s}}^\dagger h_{\bar{v}} h_{\bar{u}} - \beta \sum_{rsuv} \langle r\bar{s}|V(0)|u\bar{v}\rangle e_r^\dagger h_{\bar{s}}^\dagger h_{\bar{v}} e_u, \quad (2.11)$$

the state $|i\rangle$ represents a harmonic oscillator state defined by the quantum numbers $n_i = 0, 1, \dots$ and $l_i = -\infty, \dots, -1, 0, 1, \dots, \infty$; n and l are the radial and angular momentum quantum numbers, respectively [40]. The state $|\bar{i}\rangle$ for holes represents the same state $|i\rangle$ for electrons but with opposite sign of the angular momentum. $t_i = 2n_i + |l_i| + 1$ and $\beta = l_O/a_B$, with $a_B = \varepsilon\hbar^2/\mu e^2$ the effective Bohr radius. Finally, $\langle rs|V(0)|uv\rangle$ is the matrix element of the Coulomb interaction for charge carriers confined in the same QD, details on the explicit form and calculation of this elements can be found in Appendix A. $V(0)$ means that the charges are in the same plane, when we consider two quantum dots this condition will be relaxed and the charges might be in different planes separated by a distance a , leading to a different Coulomb element $\langle rs|V(a)|uv\rangle$, i.e., the explicit form of the potential in dimensionless units is $V(a) = 1/|\vec{r}_1 - \vec{r}_2 + \vec{a}|$, with $\vec{r}_1 \perp \vec{a}$ and $\vec{r}_2 \perp \vec{a}$.

2.3.2 $B \neq 0$

The procedure including magnetic field is pretty similar to the one developed in the previous section for $B = 0$. Instead of defining an oscillator length we define the magnetic length $l_B = \sqrt{2\hbar c/eB}$ and use the transformation to dimensionless variables $\vec{r} \rightarrow l_B\vec{r}$ and

$\vec{P} \rightarrow \frac{\hbar}{l_B} \vec{P}$. Defining the cyclotron frequency $\omega_c^{e(h)} = eB/m_{e(h)}c$ and using Coulomb's gauge for the vector potential, the hamiltonian (2.8) is written in second quantisation as [40]:

$$\begin{aligned}
H = & \sum_{kn} (t_{kn}^{(e)} e_k^\dagger e_n + t_{k\bar{n}}^{(h)} h_k^\dagger h_{\bar{n}}) + \frac{\beta}{2} \sum_{rsuv} \langle rs|V(0)|uv\rangle e_r^\dagger e_s^\dagger e_v e_u \\
& + \frac{\beta}{2} \sum_{rsuv} \langle \bar{r}\bar{s}|V(0)|\bar{u}\bar{v}\rangle h_r^\dagger h_s^\dagger h_{\bar{v}} h_{\bar{u}} - \beta \sum_{rsuv} \langle r\bar{s}|V(0)|u\bar{v}\rangle e_r^\dagger h_s^\dagger h_{\bar{v}} e_u,
\end{aligned} \tag{2.12}$$

where $t_{kn}^{e(h)} = \frac{\hbar\omega_c^{e(h)}}{2} (2n_k + |l_k| \pm l_k + 1) \delta_{kn} + \frac{\hbar\omega_c^{e(h)2}}{\omega_c^{e(h)}} \langle k|r^2|n\rangle$, with the + sign standing for electrons and the - for holes, $\langle k|r^2|n\rangle$ is the matrix element of the confining potential, and $\beta = e^2/\varepsilon l_B$. The state $|i\rangle$ represents a Landau state of a charged particle in a magnetic field. As in the harmonic oscillator case, the Landau states are defined by two quantum numbers (ignoring spin): $n_i = 0, 1, \dots$ and $l_i = -\infty, \dots, -1, 0, 1, \dots, \infty$; n and l are the radial and angular momentum quantum numbers, respectively. $\langle rs|V(0)|uv\rangle$ represents the same as in the previous section.

2.4 Light-matter interaction

The QD will be placed in a cavity where an electromagnetic field is confined. The field will interact with the dot generating excitations of matter. In this section, we will deduce the quantum expression for the light matter interaction. The latter is considered in a *dipolar approximation*, in such a way that it can be expressed as $H_{l-m} = -\vec{d} \cdot \vec{E}$, this approximation is valid if the wavelength of light is larger than the typical dimensions of the QD. The dipole moment operator is written in second quantisation formalism with field operators for electrons and holes as [23]:

$$\begin{aligned}
\vec{d} = & \int d^3r \sum_{i,j=e,h} e \psi_i^\dagger(\vec{r}) \vec{r} \psi_j(\vec{r}) \\
= & \int d^3r e \vec{r} \left[\psi_e^\dagger(\vec{r}) \psi_e(\vec{r}) + \psi_h(\vec{r}) \psi_h^\dagger(\vec{r}) + \psi_e^\dagger(\vec{r}) \psi_h^\dagger(\vec{r}) + \psi_h(\vec{r}) \psi_e(\vec{r}) \right].
\end{aligned} \tag{2.13}$$

The field operators can be expressed in terms of the creation and annihilation operators of electrons and holes defined in previous sections, and the wave functions ϕ_n of the particles, as:

$$\begin{aligned}\psi_e(\vec{r}) &= \sum_n \phi_n^e(\vec{r}) e_n & \psi_h(\vec{r}) &= \sum_n \phi_n^h(\vec{r}) h_{\bar{n}} \\ \psi_e^\dagger(\vec{r}) &= \sum_n \phi_n^{e*}(\vec{r}) e_n^\dagger & \psi_h^\dagger(\vec{r}) &= \sum_n \phi_n^{h*}(\vec{r}) h_{\bar{n}}^\dagger.\end{aligned}$$

After some calculations the obtained result is [23, Chap. 20]:

$$\vec{d} = \vec{d}_{cv} \sum_n \left(e_n^\dagger h_{\bar{n}}^\dagger + h_{\bar{n}} e_n \right), \quad (2.14)$$

where $\vec{d}_{cv} = e \int d^3r \vec{r} u_c^*(\vec{r}) u_v(\vec{r})$, with u_c and u_v Bloch functions of the bulk material of charges in the conduction and valence band, respectively.

Considering the interaction of the matter dipole with a quantised electromagnetic field and performing a *Rotating Wave Approximation* (RWA) that neglects the terms $ah_{\bar{n}}e_n$ and $a^\dagger e_n^\dagger h_{\bar{n}}^\dagger$ [19], the light-matter interaction is finally written as:

$$H_{l-m} = g \sum_n (ae_n^\dagger h_{\bar{n}}^\dagger + a^\dagger h_{\bar{n}} e_n) \quad (2.15)$$

2.5 Physical system and Hamiltonian

The system is drawn schematically in Fig. 2.3 and consists of a microcavity with light confined such that the energy levels are spaced enough to consider only one light mode. Two vertically aligned quantum dots are embedded in the cavity. Experimentally, if close enough, the layers will naturally tend to align the QDs forming vertical stacks [44, 25, 42]. The quantum dots are close enough to allow charge carriers from different dots to interact via Coulomb interaction and to allow tunnelling of particles between dots. Light matter

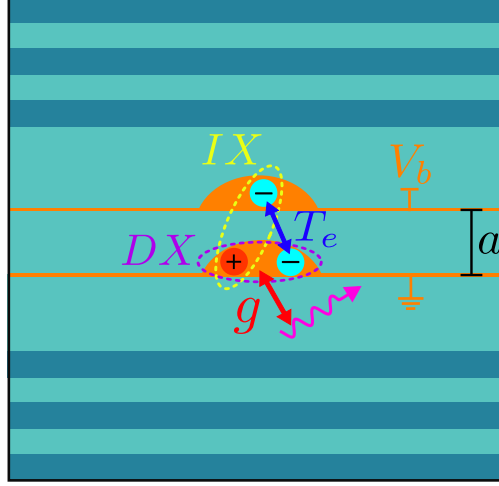


Figure 2.3: Physical system.

interaction will be in dipolar and rotating wave approximations. With this considerations, the hamiltonian of the system is as follows:

$$H = H_1^{QD} + H_2^{QD} + H_{int} + H_{tun} + H_{light}. \quad (2.16)$$

H_1^{QD} and H_2^{QD} are the hamiltonians of the charges in each quantum dot:

$$\begin{aligned} H_1^{QD} = & \sum_{kn} (t_{kn}^{(e1)} e_{k1}^\dagger e_{n1} + t_{k\bar{n}}^{(h)} h_k^\dagger h_{\bar{n}}) + \frac{\beta}{2} \sum_{rsuv} \langle r, s | V(0) | u, v \rangle e_{r1}^\dagger e_{s1}^\dagger e_{v1} e_{u1} \\ & + \frac{\beta}{2} \sum_{rsuv} \langle \bar{r}, \bar{s} | V(0) | \bar{u}, \bar{v} \rangle h_{\bar{r}}^\dagger h_{\bar{s}}^\dagger h_{\bar{v}} h_{\bar{u}} - \beta \sum_{rsuv} \langle r, \bar{s} | V(0) | u, \bar{v} \rangle e_{r1}^\dagger h_{\bar{s}}^\dagger h_{\bar{v}} e_{u1}, \end{aligned} \quad (2.17)$$

$$H_2^{QD} = \sum_{kn} t_{kn}^{(e2)} e_{k2}^\dagger e_{n2} + \frac{\beta}{2} \sum_{rsuv} \langle r, s | V(0) | u, v \rangle e_{r2}^\dagger e_{s2}^\dagger e_{v2} e_{u2}, \quad (2.18)$$

where:

$$t_{ij}^{(\alpha)} = \frac{\hbar\omega_c^\alpha}{2} (2n_i \pm l_i + |l_i| + 1) \delta_{i,j} + \frac{\hbar\omega_\alpha^2}{\omega_c^\alpha} \langle i | r^2 | j \rangle + E_{gap} \delta_{\alpha,e} \delta_{i,j} + E_0^\alpha \delta_{i,j} \quad (2.19)$$

is the energy of electrons and holes in a parabolic confinement in the presence of a magnetic field ($\alpha = e1, e2, h$) and the corresponding gap and offset (Eq. (2.7)) energies. β is the

strength of the Coulomb interaction which depends on the magnetic field. We only consider one quantum dot in strong coupling with light and include a bias voltage V_b to ensure that only electrons can tunnel, see Fig. 2.3. With this considerations, one QD will have electrons and holes and the other one will only have electrons due to tunnelling.

H_{int} is the interaction between charge carriers in different quantum dots. This interaction has a different strength γ that depends on the effective dielectric constant and the magnetic field; Coulomb matrix elements are also different due to the vertical spatial separation between the particles' wavefunctions. The quantum dots are separated by a distance a , as shown in Fig. 2.3, that defining the magnetic length $l_B = \sqrt{2\hbar c/eB}$ is transformed into a dimensionless variable $a \rightarrow l_B a$. Then, the Coulomb element for charges separated by a vertical distance a is written as $\langle r, s|V(a)|u, v\rangle$. Details on the calculation of the latter element can be found in Appendix A. H_{int} has the following form:

$$H_{int} = \gamma \sum_{rsuv} \langle r, s|V(a)|u, v\rangle e_{r1}^\dagger e_{s2}^\dagger e_{v2} e_{u1} - \gamma \sum_{rsuv} \langle r, \bar{s}|V(a)|u, \bar{v}\rangle e_{r2}^\dagger h_{\bar{s}}^\dagger h_{\bar{v}} e_{u2}. \quad (2.20)$$

While H_1^{QD} is the responsible of the formation of direct excitons (DX), H_2^{QD} jointly with H_{int} are in charge of the formation of indirect excitons (IX).

As mentioned above, a bias voltage is taken into account in order to tune the energies of electrons in the dots, and due to the opposite charge, detune the energies of holes. This tuning allows electrons only to tunnel between the QDs. The strength of the tunnelling depends on the overlapping of the wavefunctions of electrons in each dots, i.e., the separation a has a great impact in the tunnelling. Therefore, H_{tun} will be written as:

$$H_{tun} = \sum_{kn} T_{kn} (e_{k1}^\dagger e_{n2} + e_{n2}^\dagger e_{k1}), \quad (2.21)$$

where the explicit form of T_{kn} will be set according to the situation. Finally, the light hamiltonian includes the confined photons' energy and the light-matter interaction, that is:

$$H_{light} = \hbar\omega a^\dagger a + g \sum_n (a^\dagger h_{\bar{n}} e_{n1} + a e_{n1}^\dagger h_{\bar{n}}^\dagger), \quad (2.22)$$

where it is explicit that the QD labelled as 1 is the dot in strong coupling with light.

The complete hamiltonian associated to the system of Fig. 2.3 is:

$$\begin{aligned}
H = & \sum_{kn} (t_{kn}^{(e1)} e_{k1}^\dagger e_{n1} + t_{\bar{k}\bar{n}}^{(h)} h_{\bar{k}}^\dagger h_{\bar{n}} + t_{kn}^{(e2)} e_{k2}^\dagger e_{n2}) + \hbar\omega a^\dagger a \\
& + \frac{\beta}{2} \sum_{rsuv} \langle rs|V(0)|uv\rangle e_{r1}^\dagger e_{s1}^\dagger e_{v1} e_{u1} + \frac{\beta}{2} \sum_{rsuv} \langle \bar{r}\bar{s}|V(0)|\bar{u}\bar{v}\rangle h_{\bar{r}}^\dagger h_{\bar{s}}^\dagger h_{\bar{v}} h_{\bar{u}} \\
& + \frac{\beta}{2} \sum_{rsuv} \langle rs|V(0)|uv\rangle e_{r2}^\dagger e_{s2}^\dagger e_{v2} e_{u2} - \beta \sum_{rsuv} \langle r\bar{s}|V(0)|u\bar{v}\rangle e_{r1}^\dagger h_{\bar{s}}^\dagger h_{\bar{v}} e_{u1} \\
& + \gamma \sum_{rsuv} \langle rs|V(a)|uv\rangle e_{r1}^\dagger e_{s2}^\dagger e_{v2} e_{u1} - \gamma \sum_{rsuv} \langle r\bar{s}|V(a)|u\bar{v}\rangle e_{r2}^\dagger h_{\bar{s}}^\dagger h_{\bar{v}} e_{u2} \\
& + g \sum_n (a^\dagger h_{\bar{n}} e_{n1} + a e_{n1}^\dagger h_{\bar{n}}^\dagger) + \sum_{kn} T_{kn} (e_{k1}^\dagger e_{n2} + e_{n2}^\dagger e_{k1}).
\end{aligned} \tag{2.23}$$

For all the calculations in the text, we consider the QDs to be made of InGaAs with a dielectric constant $\varepsilon = 13.5$ and an energy gap $E_{gap} = 850\text{meV}$, we will ignore its temperature dependence [2]. The effective masses for electrons and holes used are $m_e = 0.05m_0$ and $m_h = 0.07m_0$, respectively, with m_0 the free electron mass. We also consider the cavity to be made of a typical material like GaAs, that has a similar dielectric constant, in such a way that we can approximate $\gamma \approx \beta$. The Rabi splitting is set to $g = 1\text{meV}$ unless stated otherwise. Other parameters such as parabolic confinement strengths or photon energy are specified in the rest of the text.

Chapter 3

Excitons in QDMs: Properties of Direct and Indirect Excitons

As mentioned in Chapter 1, dealing with many-body hamiltonians as the one in Eq. (2.23) is not easy. Several approximations are typically used in order to simplify the problem at a cost, loosing quantum correlations or neglecting interactions.

The exact diagonalization procedure allows us to solve the time-independent Schrödinger equation by truncation of an, in principle, infinite basis. In this chapter, we perform the diagonalization of the hamiltonian of electrons and holes to describe the system of two interacting QDs. We are able to obtain the energies and wave functions of the ground and excited states. The effects of the magnetic field on the state of the system are studied as well as the statistical properties of excitons.

3.1 Theory

In single quantum dots, the excitation of an electron from the valence band to the conduction band, and the respective creation of a positive charged hole in the valence band, generates the electron-hole bound state known as *exciton*; in this situation the charge carriers are both inside the QD. The tunnelling coupling present in quantum dot molecules opens the possibility of excitons with charge carriers in different QDs, this bound state is known as *indirect exciton* in order to distinguish it from the usual exciton that now will be called

direct exciton. Due to the spatial separation, the indirect excitons have a large dipole moment and longer lifetimes than the direct ones.

To study the properties of excitons in QDMs we first focus on the system without light i.e., $g = 0$ in the hamiltonian of Eq. (2.23):

$$\begin{aligned}
H = & \sum_{kn} (t_{kn}^{(e1)} e_{k1}^\dagger e_{n1} + t_{k\bar{n}}^{(h)} h_k^\dagger h_{\bar{n}} + t_{kn}^{(e2)} e_{k2}^\dagger e_{n2}) + \sum_{kn} T_{kn} (e_{k1}^\dagger e_{n2} + e_{n2}^\dagger e_{k1}) \\
& + \frac{\beta}{2} \sum_{rsuv} \langle rs|V(0)|uv\rangle e_{r1}^\dagger e_{s1}^\dagger e_{v1} e_{u1} + \frac{\beta}{2} \sum_{rsuv} \langle r\bar{s}|V(0)|u\bar{v}\rangle h_r^\dagger h_s^\dagger h_{\bar{v}} h_{\bar{u}} \\
& + \frac{\beta}{2} \sum_{rsuv} \langle rs|V(0)|uv\rangle e_{r2}^\dagger e_{s2}^\dagger e_{v2} e_{u2} - \beta \sum_{rsuv} \langle r\bar{s}|V(0)|u\bar{v}\rangle e_{r1}^\dagger h_s^\dagger h_{\bar{v}} e_{u1} \\
& + \gamma \sum_{rsuv} \langle rs|V(a)|uv\rangle e_{r1}^\dagger e_{s2}^\dagger e_{v2} e_{u1} - \gamma \sum_{rsuv} \langle r\bar{s}|V(a)|u\bar{v}\rangle e_{r2}^\dagger h_s^\dagger h_{\bar{v}} e_{u2}.
\end{aligned} \tag{3.1}$$

To perform the diagonalization of the hamiltonian (3.1) we must first choose a “good” basis to find the matrix form of the hamiltonian [47]. As mentioned in Section 2.3.2, the state of a charged particle in the presence of a magnetic field (Landau state) is defined by two quantum numbers: the angular momentum l and the radial quantum number n . In the case of zero magnetic field, the particles are still subject to a parabolic confinement potential; the eigenstates for this situation (2D Harmonic oscillator states) are defined by the same quantum numbers l and n , indeed, the eigenfunctions in the position basis are the same (see Appendix A). These bases will be used in accordance to the situation. We will consider the quantum dots to be made of InGaAs, which is a material with a direct band gap, thus, when the material is excited the electron in the conduction band will have the same angular momentum as the hole in the valence band, with opposite sign due to the opposite charge; the electron-hole pair state will have total angular momentum zero [46], this constrain will remain in the interacting case since Coulomb interaction preserves the angular momentum and the tunnelling is considered elastic.

We proceed to construct states $|S_{e1}\rangle |S_{e2}\rangle |S_h\rangle$ with zero total angular momentum and equal number of electrons and holes [46, 47, 50]. $|S\rangle$ represents a Slater determinant of single particle states of electrons in each dot or holes. Each state constructed this way will have an integer number of electron-hole pairs, this means that the hamiltonian without light will be diagonalized for a fixed number of excitons, this can be done because the operator in Eq. (3.1) commutes with the number of excitons [50] defined as:

$$N_{exc} = \frac{1}{2} \sum_n (e_{n1}^\dagger e_{n1} + e_{n2}^\dagger e_{n2} + h_n^\dagger h_{\bar{n}}). \quad (3.2)$$

We construct all the states for a fixed number of excitons, calculate the matrix form of the hamiltonian in this basis and realize the numerical diagonalization, the lowest eigenvalue represents the ground-state energy and the corresponding linear combination of states used for the diagonalization will be the ground-state ket, similarly, the excited states are obtained.

It is important to notice that both the Landau and 2D harmonic oscillator bases are infinite, so they must be truncated at a certain l_{max} and n_{max} . This truncation is, in principle, due to computational reasons, however, it is also natural for the system since states with a large angular momentum and energy will overcome the confinement in the QD and leave. The 2D Harmonic oscillator basis will be used for the $B = 0T$ situation and the Landau basis otherwise, we note that at low magnetic fields ($B \approx 1 - 3T$) some precision may be lost due to the finite Landau basis, but the qualitative behaviour remains.

3.2 Effects of magnetic field on a single exciton

The exact diagonalization of the hamiltonian from Eq. (3.1) was performed using a basis constructed as explained in the previous section and composed of 120 single particle (Landau) states, distributed in 3 levels, i.e., $n_{max} = 2$. We set $N_{exc} = 1$. The strengths of the parabolic confinements were taken as $\hbar\omega_h = 8\text{meV}$, $\hbar\omega_{e1} = 12\text{meV}$ and $\hbar\omega_{e2} = 18\text{meV}$, and the separation between dots as $a = 10\text{nm}$. The corresponding energy offsets due to the confinement in the z direction (Eq. (2.7)) were fixed at $E_0^h = 10\text{meV}$, $E_0^{e1} = 15\text{meV}$ and E_0^{e2} was set such that, by means of the electric field, the single particle electron state with quantum numbers $n = 0$ and $l = 0$, in both quantum dots, are tuned at the same energy.

First, we ignore the tunnelling and plot the energies of the DX and IX for several values of magnetic field, the results are depicted in Fig. 3.1. We see that while the IX energy increases monotonically with B , the DX energy has a richer behaviour. At low values of the magnetic field ($B < 5T$) the Coulomb interaction gives a relevant contribution $\sim -\sqrt{B}$ that decreases the energy [49]. As the field increases, the contribution of the Landau energy $\sim \hbar\omega_c \propto B$ becomes more relevant than the Coulomb interaction and the energy

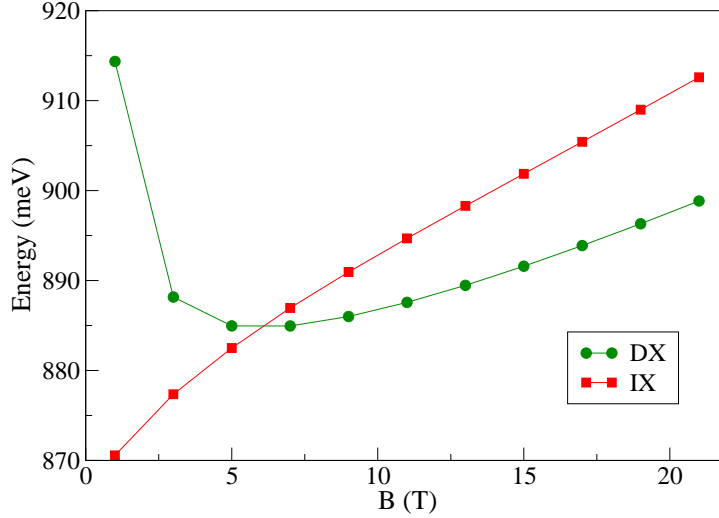


Figure 3.1: Energy of the IX and DX as a function of the magnetic field.

starts increasing, causing a change in the slope. The IX has a simpler behaviour due to the spatial separation of the charge carriers that reduces the Coulomb matrix elements and the effect of Coulomb's interaction is lost.

In order to include tunnelling we have to set the rate T_{kn} . This zero temperature treatment allows us to ignore effects from lattice vibrations (phonons) and consider the tunnelling to be completely elastic [45, 36, 43], such that the tunnelling will occur between the level that is tuned in the dots. This state, as mentioned above, is defined by the quantum numbers $n = 0$ and $l = 0$, and we label it as the state number 1, which lets us write the tunnelling rate as $T_{kn} = T_e \delta_{n,k} \delta_{k,1}$.

In Fig. 3.2 we plot the energy and composition of the ground and first excited state of the hamiltonian from Eq. (3.1) for several values of the magnetic field, the tunnelling rate was fixed at $T_e = 3\text{meV}$. The expected avoided crossing between the energies of Fig. 3.1 is found. The composition of the ground state follows a behaviour that can be expected from the results from Fig. 3.1. At small values of the magnetic field the IX has lower energy than the DX, for this reason the ground state is highly composed of IX. As the field increases, the DX and IX have similar energies and the ground state becomes a superposition of the two kinds of excitons. Finally, at high magnetic fields, the DX has lower energy compared

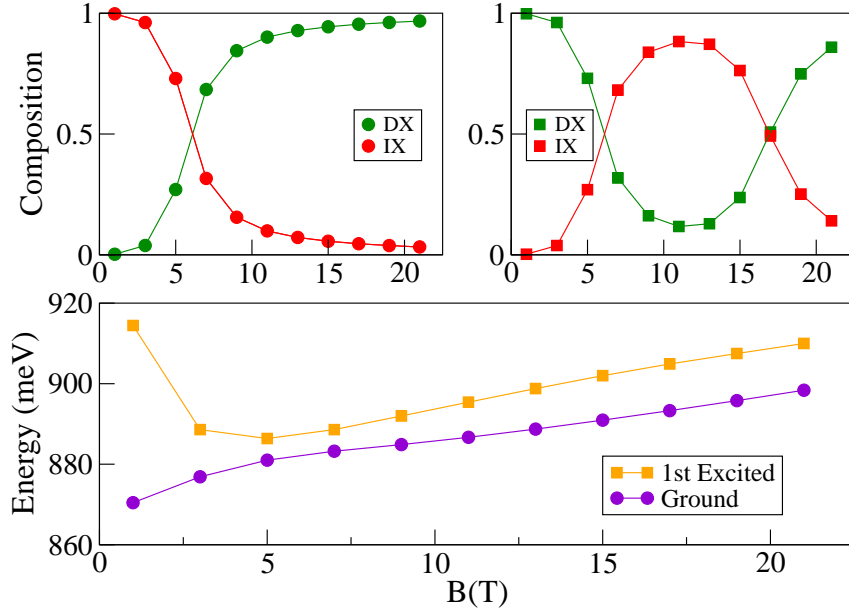


Figure 3.2: Energy and composition of the ground (circles) and first excited (squares) state, as a function of the magnetic field, for the system without light.

to the IX and becomes the most relevant contribution on the composition. A similar analysis can be performed for the first excited state but there is something to note for $B > 15\text{T}$. The IX composition of the state decreases while the DX counterpart increases, this occurs because the IX exceeds the energy of another excited state of the DX branch (DX+).

3.3 Statistics of exciton operators

When quasiparticle operators are defined, the commutation relation they follow is of great interest since many-body properties are strongly affected by (quasi)particles statistics. If the quasiparticle operators are not defined by a unitary transformation (e.g, Bogoliubov transformation), the commutation relations are not trivial and may be affected by the system parameters [32]. In this section we will study the statistics of the exciton operators.

We consider one quantum dot which may confine up to 1 electron-hole pair. At this moment we are not interested in quantitative accuracy, so for the sake of simplicity we will consider electron's and hole's effective masses to be the same μ . Also, the particles will be subject to the same parabolic confinement $\hbar\omega_0$. The hamiltonian which describes this system, in units of $\hbar\omega_0$, can be written as:

$$\frac{H_{eh}}{\hbar\omega_0} = \sum_n t_n (e_n^\dagger e_n + h_{\bar{n}}^\dagger h_{\bar{n}}) - \beta \sum_{rsuv} \langle r\bar{s}|V(0)|u\bar{v}\rangle e_r^\dagger h_{\bar{s}}^\dagger h_{\bar{v}} e_u. \quad (3.3)$$

We will shut-down the magnetic field for this calculation such that the state $|n\rangle$ will denote a 2D harmonic oscillator state and $t_n = 2n_n + |l_n| + 1$ (it is easy to distinguish the state's index and the principal quantum number even if both are labelled as n). Defining the oscillator length $l_O = \sqrt{\hbar/\mu\omega_0}$ we have made the Coulomb matrix elements dimensionless. The strength of the Coulomb interaction is $\beta = l_O/a_B$, with $a_B = \epsilon\hbar^2/\mu e^2$ the effective Bohr radius [40].

The eigenstates $|DX_i\rangle$ of the hamiltonian (3.3) are the direct exciton states, we assume they are orthonormal $\langle DX_i|DX_j\rangle = \delta_{ij}$. To avoid ambiguity, the exciton states are denoted with the indices i, j and the single particle states are denoted by the other indices different from i and j .

We define b_i^\dagger the operator that creates a direct exciton in the state i , such that $b_i^\dagger |0\rangle = |DX_i\rangle$. Taking into account that $e_n^\dagger h_{\bar{m}}^\dagger |0\rangle = |n\bar{m}\rangle$ and the completeness relation of the single particle bases $\sum_n |n\rangle \langle n| = 1$, we can write the exciton operators as [11]:

$$b_i = \sum_{nm} \langle DX_i|n\bar{m}\rangle h_{\bar{m}} e_n, \quad b_i^\dagger = \sum_{nm} \langle n\bar{m}|DX_i\rangle e_n^\dagger h_{\bar{m}}^\dagger. \quad (3.4)$$

We now proceed to the calculation of the commutator between b_i and b_i^\dagger using the commutation relations of electron and hole operators:

$$\begin{aligned}
[b_i, b_i^\dagger] &= \sum_{kpnm} \langle DX_i | n\bar{m} \rangle \langle k\bar{p} | DX_i \rangle e_n h_{\bar{m}} h_{\bar{p}}^\dagger e_k^\dagger - \sum_{kpnm} \langle DX_i | n\bar{m} \rangle \langle k\bar{p} | DX_i \rangle e_k^\dagger h_{\bar{p}}^\dagger h_{\bar{m}} e_n \\
&= \sum_{kpnm} \langle DX_i | n\bar{m} \rangle \langle k\bar{p} | DX_i \rangle \left\{ (\delta_{nk} - e_k^\dagger e_n) (\delta_{pm} - h_{\bar{p}}^\dagger h_{\bar{m}}) - e_k^\dagger e_n h_{\bar{p}}^\dagger h_{\bar{m}} \right\} \\
&= 1 - \sum_{knm} \langle DX_i | n\bar{m} \rangle \langle k\bar{m} | DX_i \rangle e_k^\dagger e_n - \sum_{pnm} \langle DX_i | n\bar{m} \rangle \langle n\bar{p} | DX_i \rangle h_{\bar{p}}^\dagger h_{\bar{m}}. \quad (3.5)
\end{aligned}$$

In order to have an idea of the order of magnitude of the terms that deviate the commutation rule from the pure bosonic one, we calculate the mean value of the commutator in the state $|DX_i\rangle$ and obtain:

$$\begin{aligned}
\langle [b_i, b_i^\dagger] \rangle &= 1 - \left(\sum_{knm} |\langle DX_i | n\bar{m} \rangle \langle k\bar{m} | DX_i \rangle|^2 + \sum_{pnm} |\langle DX_i | n\bar{m} \rangle \langle n\bar{p} | DX_i \rangle|^2 \right) \\
\langle [b_i, b_i^\dagger] \rangle &= 1 - D. \quad (3.6)
\end{aligned}$$

The deviation D will set the statistics of the excitons. It is clear that if the excitons are bosons, the commutator must be 1, let us see what happens if they are fermions. Let us consider two fermion operators σ_i and σ_i^\dagger , $\{\sigma_i, \sigma_j^\dagger\} = \delta_{ij}$. Their commutator is:

$$[\sigma_i, \sigma_i^\dagger] = 1 - 2\sigma_i^\dagger \sigma_i. \quad (3.7)$$

If we take the mean value of the commutator in a state $|DX_i\rangle$ of a single exciton we obtain:

$$\langle [\sigma_i, \sigma_i^\dagger] \rangle = -1. \quad (3.8)$$

The criteria developed establishes that if the direct exciton operators follow Bose statistics, the deviation D should approach 0 and the commutator 1, moreover, if the direct exciton

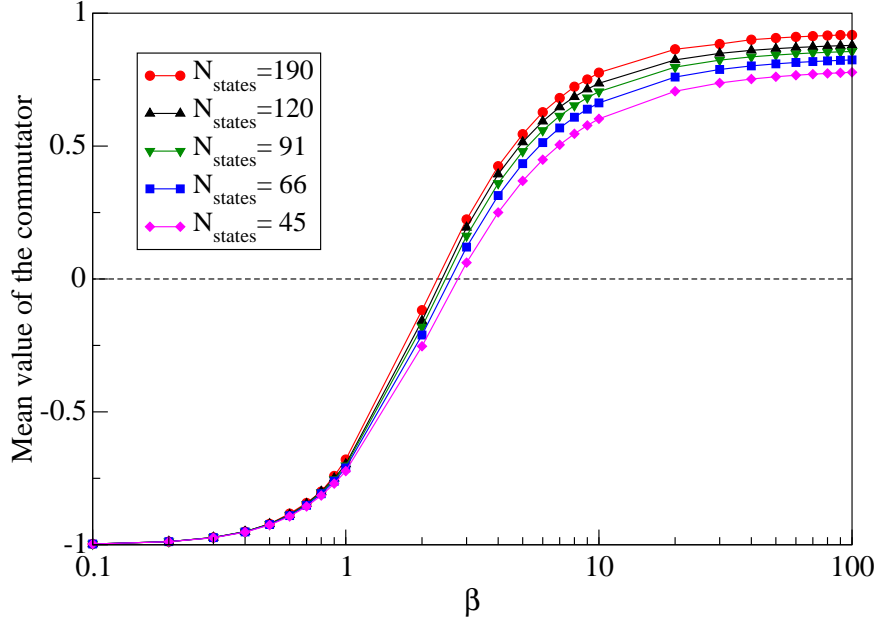


Figure 3.3: Mean value of the exciton operators' commutator as a function of the Coulomb interaction strength, for several sizes of the basis.

operators follow Fermi statistics, the deviation D should approach 2 and the commutator -1.

Fig. 3.3 shows the dependence of the mean value of the commutator (Eq. (3.6)) with β , the state $|DX_i\rangle$ used in the calculations was the ground state of the hamiltonian (3.3) for 1 electron-hole pair. Several sizes of the basis (N_{states}) were used to show the convergence, although computational restrictions did not allow us to increase the basis enough to reach good convergence at high values of β , where the harmonic oscillator basis is not convenient because the parabolic confinement takes a small value, it is clear that in this regime the commutator tends to 1 and the excitons tend to behave like bosons, this situation corresponds to large quantum dots [38] in which the overlapping between excitons' wavefunctions is negligible [32]. On the other hand, for small values of β (large values of $\hbar\omega_0$), the Coulomb interaction is negligible compared to the confinement and the fermionic nature of electrons and holes becomes relevant. We also note that the transition between the regimes is pronounced when $l_O \sim a_B$. This result is consistent with that in

Ref. [32] where the authors analyse the matrix elements of the operator b^\dagger to determine the statistics.

A similar procedure can be developed for indirect excitons IX and the result should be alike. When $\hbar\omega_0$ is large, the strength of Coulomb interaction γ decreases at the same rate as the direct exciton one, however, the dimensionless separation between quantum dots a takes a large value (because l_O becomes small), causing the interaction matrix elements $\langle rs|V(a)|uv\rangle$ to be smaller than those of the DX case; the final result is a negligible Coulomb interaction compared to the confinement, making the IXs to behave as fermions faster than DXs. At the other limit, in which $\hbar\omega_0$ is small, the dimensionless separation between dots decreases ($a \ll 1$) and the interaction matrix elements tend to those of the DX case: $\langle rs|V(a)|uv\rangle \approx \langle rs|V(0)|uv\rangle$; the IXs will behave as bosons just like the DXs do. In conclusion, the mean value of the commutator of indirect exciton operators should behave like Fig. 3.3 but with a sharper transition at $l_O \sim a_B$.

Chapter 4

Dipolaritons in QDs: Exact Diagonalization

An optical emitter inside a microcavity that confines light may reach a strong coupling regime. In this regime, the interaction between excitons and photons gives rise to new quantum states of the light-matter coupled system known as *polaritons* [31]. The photon component provides polaritons with a small effective mass (around 10^{-4} times the bare electron mass) and, since photons may leak from the cavity, a lifetime (between 1 – 100ps). Instead, the exciton component provides the polariton-polariton interactions that are inherited mainly from the Coulomb interaction between excitons [9].

In a system of two coupled emitters, when light-matter interaction is included, a new kind of polaritons arise. Light couples with matter via direct exciton, and the latter couples with the indirect exciton via tunnelling. The collective modes of this interactions are known as *dipolaritons*, quasiparticles found experimentally by Cristofolini *et al.* in QWs, they are basically polaritons with a large dipole moment due to their indirect exciton component. All the research that has been made around dipolaritons, to the best of our knowledge, has focused on QW systems, in this chapter we extend this idea to zero dimensional systems and propose the existence of dipolaritons in quantum dots.

4.1 Theory

In the previous chapter, the exact diagonalization method was used to investigate both direct and indirect excitons' features. Now we extend this procedure to take light-matter interaction into account for the generation of dipolaritons.

To study the properties of dipolaritons in QDs, the full hamiltonian (2.23) is taken into account. This hamiltonian commutes with the number of dipolaritons operator defined as [47, 50]:

$$N_{dip} = N_{ph} + N_{exc} = a^\dagger a + \frac{1}{2} \sum_n (e_{n1}^\dagger e_{n1} + e_{n2}^\dagger e_{n2} + h_{\bar{n}}^\dagger h_{\bar{n}}), \quad (4.1)$$

for this reason, we can perform the diagonalization of the hamiltonian for a fixed number of dipolaritons. We construct a basis similar to the one used in the previous chapter but including a Fock state for the light $|N_{ph}\rangle |S_{e1}\rangle |S_{e2}\rangle |S_h\rangle$. We set, also, a maximum number of excitons in the system N_{exc}^{max} because the quantum dots are finite and have a limit on the charge carriers they can confine [47]. Thus, we construct all the possible states that satisfy $N_{ph} + N_{exc} = N_{dip}$ with N_{exc} ranging from 1 to N_{exc}^{max} .

4.2 Dipolariton modes

Constructing the basis for $N_{dip} = 1$ with the Fock state for the photons having the possibilities $N_{ph} = 0$ or $N_{ph} = 1$, and using 120 single particle states distributed in 3 Landau levels, we diagonalized the hamiltonian (2.23). The tunnelling was taken as described in the previous chapter with $T_e = 3\text{meV}$. The strengths of the parabolic confinements used were $\hbar\omega_h = 8\text{meV}$, $\hbar\omega_{e1} = 12\text{meV}$ and $\hbar\omega_{e2} = 18\text{meV}$. The energies of the offsets due to the confinement in the z direction were fixed at the same values used in Chapter 3 with E_0^{e2} such that, by means of the electric field, the single particle electron state with quantum numbers $n = 0$ and $l = 0$, in both quantum dots, are tuned at the same energy.

The first four eigenenergies of the system and the composition of the corresponding eigenstate as a function of the photon energy are plotted in Fig. 4.1. The bare energies of the photon C, indirect exciton IX and direct exciton DX are plotted with dashed lines as a reference. As in Ref. [13], the three dipolariton branches are recognized. The avoided

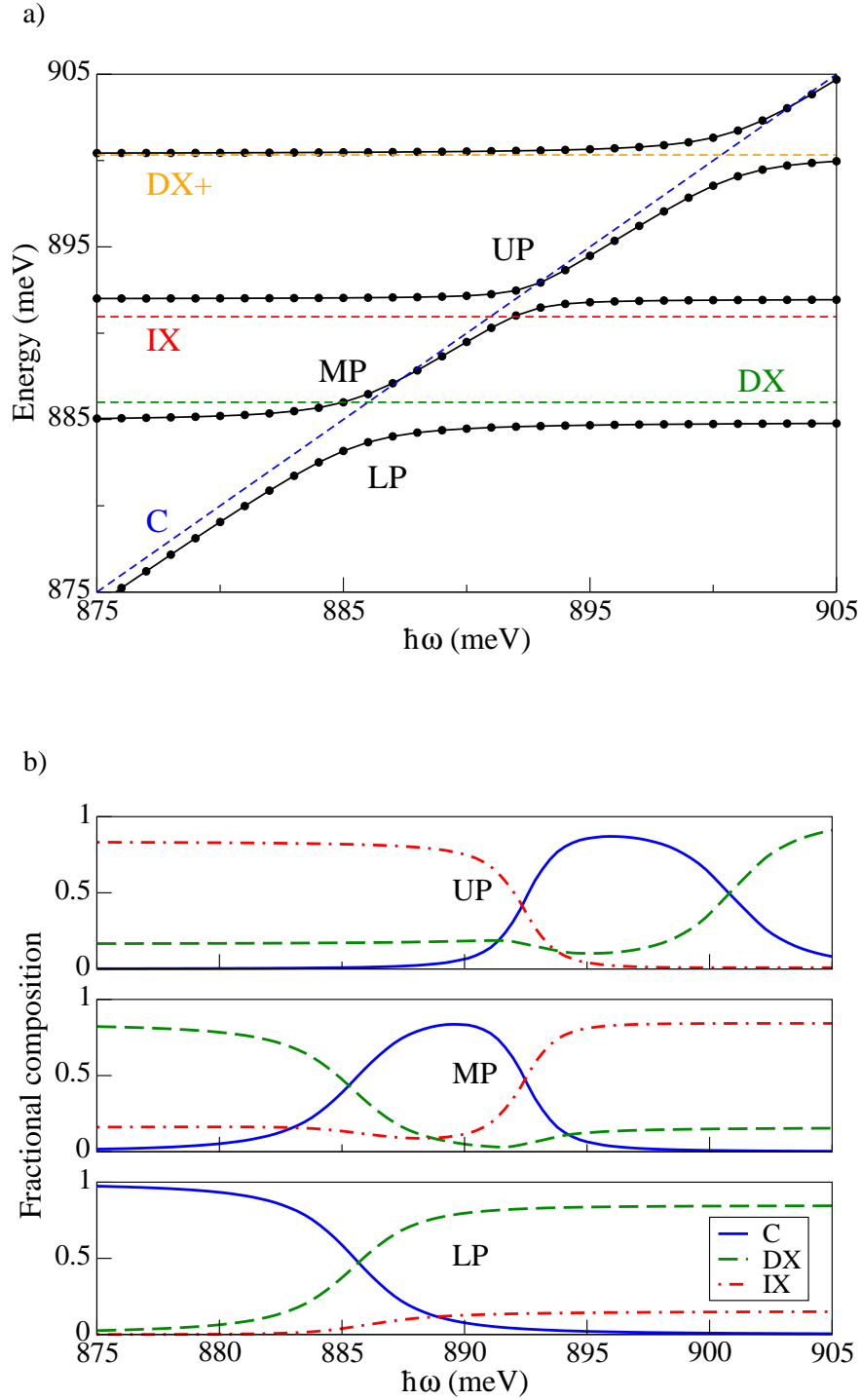


Figure 4.1: a) First four eigenenergies of the hamiltonian from Eq. (2.23) (black), bare energies of the photon (blue), indirect exciton (red), direct exciton (green) and second excited of the direct exciton (orange); as a function of the photon energy. b) Composition of the three dipolariton branches as a function of the photon energy. The magnetic field was fixed at $B=9T$.

crossing between the *lower dipolariton* LP and *middle dipolariton* MP branches occurs due to the light-matter interaction. The anticrossing between the MP and the *upper dipolariton* UP branches has the same reason, however, this splitting is reduced due to the tunnelling because the IX does not couple with light. From the composition of the dipolariton branches we can see that the optical detuning determines if the electron spends more time shuttling between QDs or Rabi flopping on the DX transition [13], e.g., for $\hbar\omega > 887\text{meV}$, the LP spends more time oscillating between DX and IX but for $\hbar\omega < 887\text{meV}$, the LP tends to perform Rabi oscillations.

Effective models like the ones used in Refs. [13], [28] and [10] cannot predict the avoided crossing between the UP and a higher energy branch shown in Fig. 4.1a. Compare, for example, with Fig. 1.7 where the independent variable is the indirect exciton's energy. Our model allows us to have access to higher excited states of the excitons, in particular, of the direct exciton (DX+), this anticrossing causes the UP to increase its composition of DX for high values of the photon energy (Fig. 4.1b), exhibiting the limitations of effective models.

4.3 Effects of magnetic field on a single dipolariton

To see the effects of the magnetic field on a single dipolariton, we plot the energy of the ground state and the first excited state as a function of the magnetic field, the results are shown in Fig. 4.2. The parameters used are the same of the previous section. The energy of the light does not depend on the magnetic field while the energy of the superposition of DX and IX increases with the field; at $B \sim 7\text{T}$ both energies are near resonance and the light-matter interaction causes an avoided crossing.

The composition of the ground state and the first excited are plotted in the upper panels of Fig. 4.2. At low B , the ground state is completely composed of IX, in contrast, the first excited is completely composed of light. Increasing the field, the composition of the states can be controlled to become a mixture of the three modes: IX, DX and C. Finally, at high values of the magnetic field, the matter acquires higher energy than light and the ground state becomes highly photon populated.

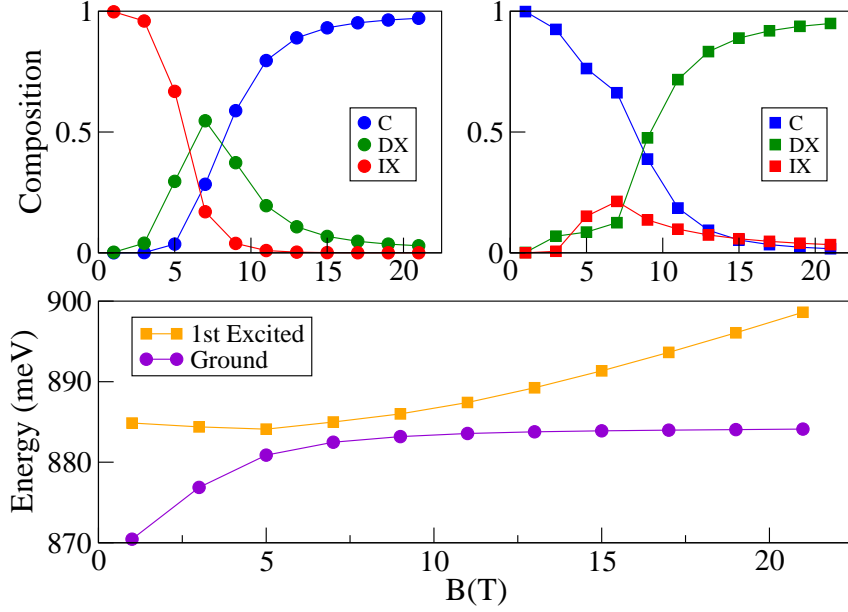


Figure 4.2: Energy and composition of the ground state (circles) and the first excited (squares), as a function of the magnetic field, for the system with light. The light energy was set to $\hbar\omega = 885\text{meV}$.

4.4 Emission

Semiconductor systems are interesting for its emission properties that can be used for the implementation of lasers and single photon sources. Emission occurs when photons leak through cavity mirrors, this means that the hamiltonian treatment developed here cannot describe this dissipative process. Usually, dissipative terms written in a Lindblad form are used in a master equation to take account dissipation and the emission is calculated with the Fourier transform of the first-order correlation function [31], but if the interest is not on the full spectrum but in more specific information as the height and position of the intensity peak our hamiltonian treatment is enough.

The intensity of the emission can be obtained from the probability of annihilating a photon:

$$I \sim |\langle N_{dip} - 1 | a | N_{dip} \rangle|^2, \quad (4.2)$$

where $|N_{dip}\rangle$ and $|N_{dip} - 1\rangle$ denote a state with dipolariton number N_{dip} and $N_{dip} - 1$, respectively. We assume that the system is operating at low temperatures, then the initial state is the ground state of the N_{dip} system [47]. From the computation of Eq. (4.2) we find that the transition to the ground state of the $N_{dip} - 1$ system is the only one that gives a significant contribution to the intensity.

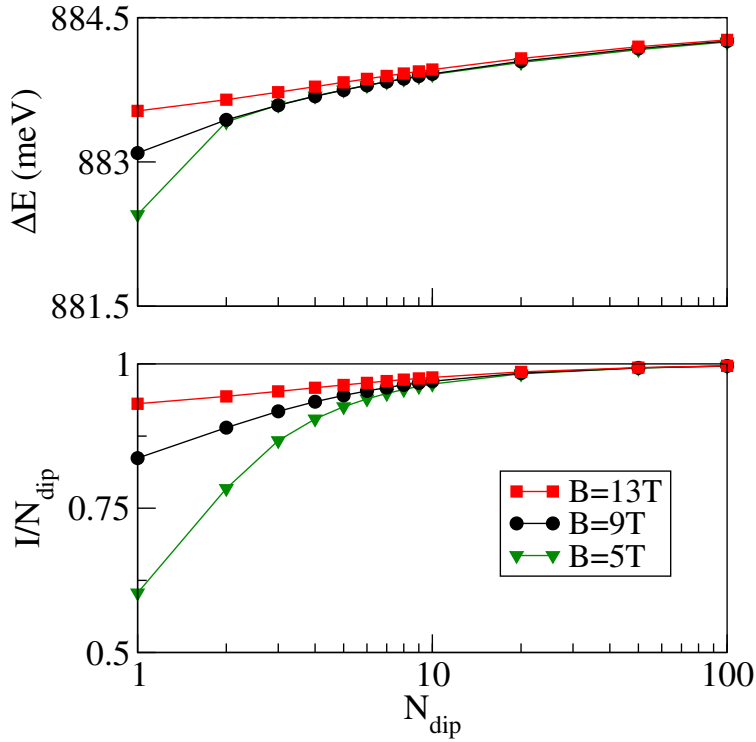


Figure 4.3: Upper panel: Energy position of the emission line as a function of the dipolariton number, $\Delta E = E(N_{dip}) - E(N_{dip} - 1)$. Lower panel: Relative intensity as a function of the dipolariton number. $\hbar\omega_h = 5\text{meV}$, $\hbar\omega_{e1} = 7\text{meV}$, $\hbar\omega_{e2} = 8\text{meV}$ and $\hbar\omega = 884.5\text{meV}$.

The position and intensity of the emission line as a function of N_{dip} for several values of B are calculated from Eq. (4.2) and depicted in Fig. 4.3. The number of electron-hole

pairs (N_{exc}) is restricted to a maximum of one. As expected, at the limit $N_{dip} \gg N_{exc}$, light is emitted at bare photon energies and $I \approx N_{dip}$ [47]. When $N_{dip} \sim N_{exc}$ the excitons enhance the trapping of light, decreasing the intensity of the emission, also, the emission is red-shifted due to light-matter interaction. At $B = 5T$ the system is in resonance, the emission is minimum and highly red-shifted. As B increases, the DX becomes detuned from the photons, which reduces the red-shift and emission is less inhibited.

Chapter 5

Multiexcitonic QDs: Zero Temperature Variational Method

Although the exact diagonalization procedure allows us to have control over the number of particles in the system and gives us access to the excited states, it becomes computationally infeasible if we want to study a large number of dipolaritons (>3). The variational method is a good option to deal with this inconvenience and obtain an approximation of the ground-state of the system.

In this chapter, we model the system of two large quantum dots which are able to confine more than 1 electron-hole pair (*multiexcitonic QDs*). A variational method is performed to find an approximation of the ground-state physics. The effects of the magnetic field and number of dipolaritons in the system are determined. Also, the statistical properties of exciton operators are revised and compared with the results obtained in Chapter 3.

5.1 Theory

Based on the variational method developed for excitons and polaritons in Refs. [14], [39] and [49], we use an extension of a BCS-like state as a trial function:

$$|\sigma, u_n, v_n, w_n\rangle = |\sigma\rangle \otimes \prod_n^{N_{states}} (u_n + v_n e_{n1}^\dagger h_{\bar{n}}^\dagger + w_n e_{n2}^\dagger h_{\bar{n}}^\dagger) |0\rangle, \quad (5.1)$$

where $|\sigma\rangle$ represents a coherent state of light, v_n^2 (w_n^2) is the probability of having a direct (indirect) electron-hole pair in the state n and N_{states} is the number of states we consider in our finite basis. The normalization condition of the BCS-like function is $u_n^2 + v_n^2 + w_n^2 = 1$.

The mean value of the hamiltonian (2.23) is calculated using the trial function from Eq. (5.1) with the help of Wick's theorem [40], and setting the commutation rules $\{e_i, h_{\bar{j}}\} = 0$, $\{e_{i1}, e_{j2}\} = 0$. We model the tunnelling as $T_{kn} = T_e \delta_{kn}$, such that electrons will tunnel to the same level in the QDs. By minimizing $\langle H \rangle$ with respect to σ , v_n and w_n , imposing the constrain of fixed number of dipolaritons, we obtain the following generalized gap equations [49]:

$$\Delta_n = g\sigma - \beta \sum_{k \neq n} \langle kn|V(0)|nk\rangle u_k v_k, \quad (5.2)$$

$$\Omega_n = T_e - \gamma \sum_{k \neq n} \langle kn|V(a)|nk\rangle v_k w_k, \quad (5.3)$$

$$\Gamma_n = -\gamma \sum_{k \neq n} \langle kn|V(a)|nk\rangle u_k w_k, \quad (5.4)$$

and the following set of equations for the variational parameters:

$$2(\varepsilon_n^{(1)} - \mu/2)u_n v_n + \Delta_n(u_n^2 - v_n^2) - \Gamma_n v_n w_n + \Omega_n u_n w_n = 0, \quad (5.5)$$

$$2(\varepsilon_n^{(2)} - \mu/2)u_n v_n - \Delta_n v_n w_n + \Gamma_n(u_n^2 - w_n^2) + \Omega_n u_n v_n = 0, \quad (5.6)$$

$$(\hbar\omega - \mu)\sigma + g \sum_n u_n v_n = 0. \quad (5.7)$$

Eqs. (5.5) and (5.6), with the normalization condition, yield to more than one solution for u_n , v_n and w_n , we choose the one that minimizes energy. The explicit expression for the mean number of dipolaritons is:

$$\bar{N}_{dip} = |\sigma|^2 + \sum_n (v_n^2 + w_n^2), \quad (5.8)$$

μ is the chemical potential which arises as a Lagrange multiplier associated to the conservation of \bar{N}_{dip} ; and, $\varepsilon_n^{(1)}$ and $\varepsilon_n^{(2)}$ are the direct and indirect pair energies, respectively, defined as:

$$\begin{aligned} \varepsilon_n^{(1)} = & \frac{1}{2}(t_{nn}^{(e1)} + t_{nn}^{(h)}) - \frac{\beta}{2} \langle nn|V(0)|nn\rangle \\ & - \frac{\beta}{2} \sum_{k \neq n} \langle kn|V(0)|nk\rangle w_k^2 - \beta \sum_{k \neq n} \langle kn|V(0)|nk\rangle v_k^2, \end{aligned} \quad (5.9)$$

$$\begin{aligned} \varepsilon_n^{(2)} = & \frac{1}{2}(t_{nn}^{(e2)} + t_{nn}^{(h)}) - \frac{\gamma}{2} \langle nn|V(a)|nn\rangle - \frac{\beta}{2} \sum_{k \neq n} \langle kn|V(0)|nk\rangle v_k^2 \\ & - \beta \sum_{k \neq n} \langle kn|V(0)|nk\rangle w_k^2 + \sum_{k \neq n} \langle kn|[\beta V(0) - \gamma V(a)]|kn\rangle w_k^2. \end{aligned} \quad (5.10)$$

Eqs. (5.2)-(5.10) are to be iteratively solved until two successive iterations yield the same probabilities v_n^2 and w_n^2 , chemical potential μ and photon number $|\sigma|^2$, to the desired accuracy [6].

5.2 Effects of magnetic field on multiexcitonic QDMs

We consider bigger quantum dots that can confine several excitons, this is manifested in smaller values of the parabolic confinement [38]: $\hbar\omega_h = 0.5\text{meV}$, $\hbar\omega_{e1} = \hbar\omega_{e2} = 1\text{meV}$. Light frequency is set to $\hbar\omega = 860\text{meV}$ and light-matter interaction to $g = 1\text{meV}$. We consider the QDs to be separated by a distance $a = 15\text{nm}$ and assume a tunnelling rate $T_e = 2\text{meV}$. The offsets are fixed at: $E_0^{e1} = 10\text{meV}$ and $E_0^h = 7\text{meV}$, and E_0^{e2} was taken as in the previous chapters. The iterative procedure described in the previous section is computed for several values of the magnetic field and number of dipolaritons.

Fig. 5.1 shows the dependence of the number of photons with the magnetic field and dipolariton number. For a fixed number of dipolaritons, N_{ph} decreases at low values of the magnetic field, when the detuning between matter and light is small. At high values of B , the energy of the excitons increase and the system is detuned, causing the state to be highly photon populated.

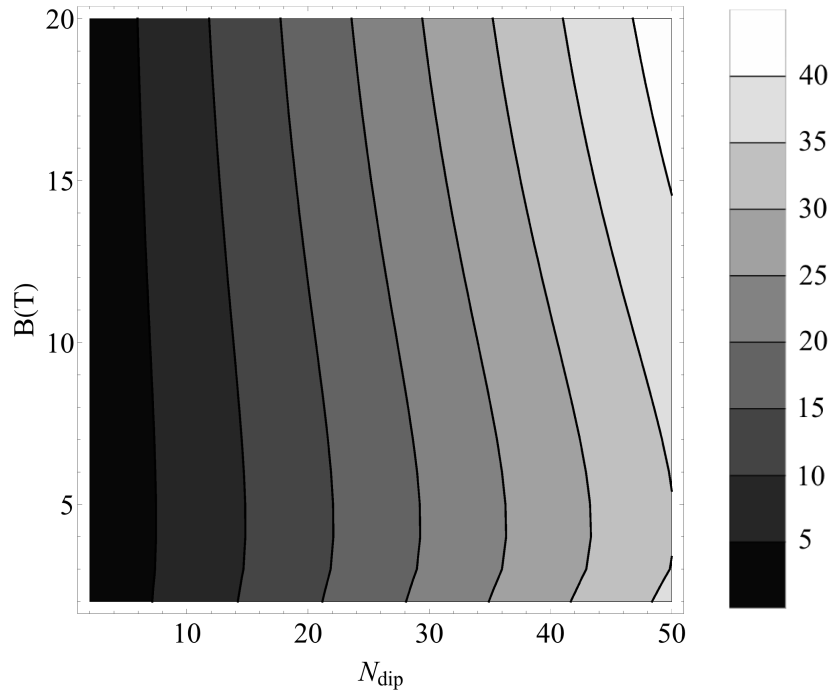


Figure 5.1: Number of photons vs the magnetic field and dipolariton number.

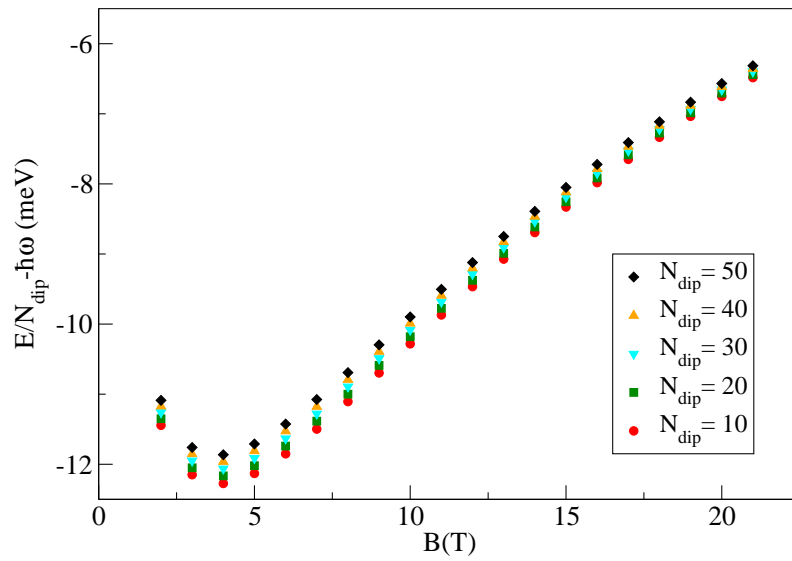


Figure 5.2: Scaling of the total energy as a function of the magnetic field.

The energy of the system, measured with respect to the bare photon energy, as a function of the magnetic field, is displayed in Fig. 5.2. In contrast with Fig. 3.1, for the parameters used the IX has higher energy than the DX, this causes the ground state of the system to have a high component of direct excitons. Therefore, as in Fig. 3.1, the energy of the DXs decreases at low B , causing the total energy to also diminish, but for $B > 5\text{T}$ the IXs and DXs' energy augments, and the total energy of the system rises. As in Ref. [49] for polaritons, we find the scaling $E \sim N_{dip}$ as an indicator that the effective interactions between dipolaritons are weak; also, as in the same reference, we find that the scaling is completely natural at high magnetic fields as happens for excitons [33]. The change in the slope means that at low B the system has a paramagnetic response but at high magnetic fields has a diamagnetic response.

5.3 Statistics of exciton operators

The variational method developed gives us also the possibility to study the statistics of excitonic operators. To do so, we will focus in direct excitons only ($T_{kn} = 0$, $\gamma = 0$), such that $w_n = 0$ in the trial wavefunction from Eq. (5.1), and we will ignore light-matter interaction ($g = 0$) and the magnetic field ($B = 0$). Electrons and holes will have the same effective mass μ and will be subject to the same parabolic confinement $\hbar\omega_0$. Similarly to the procedure developed in Sec. 3.3, we define the direct exciton's operators s_i^\dagger and s_i that satisfy $s_i^\dagger |0\rangle = |dx_i\rangle$ and $s_i |dx_i\rangle = |0\rangle$. The ket $|dx_i\rangle$ denotes a BCS state with a mean number of 1 direct exciton, in contrast to $|DX_i\rangle$ that denotes a Fock state of 1 exciton; this fact distinguishes s_i and s_i^\dagger from the operators b_i and b_i^\dagger defined in Chapter 3. Thus, we write the state as:

$$|dx_i\rangle = \prod_{n=1}^{N_{states}} (u_n + v_n e_n^\dagger h_n^\dagger) |0\rangle, \quad (5.11)$$

and the operators as:

$$s_i = \sum_{nm} \langle dx_i | n\bar{m} \rangle h_{\bar{m}} e_n, \quad s_i^\dagger = \sum_{nm} \langle n\bar{m} | dx_i \rangle e_n^\dagger h_{\bar{m}}^\dagger. \quad (5.12)$$

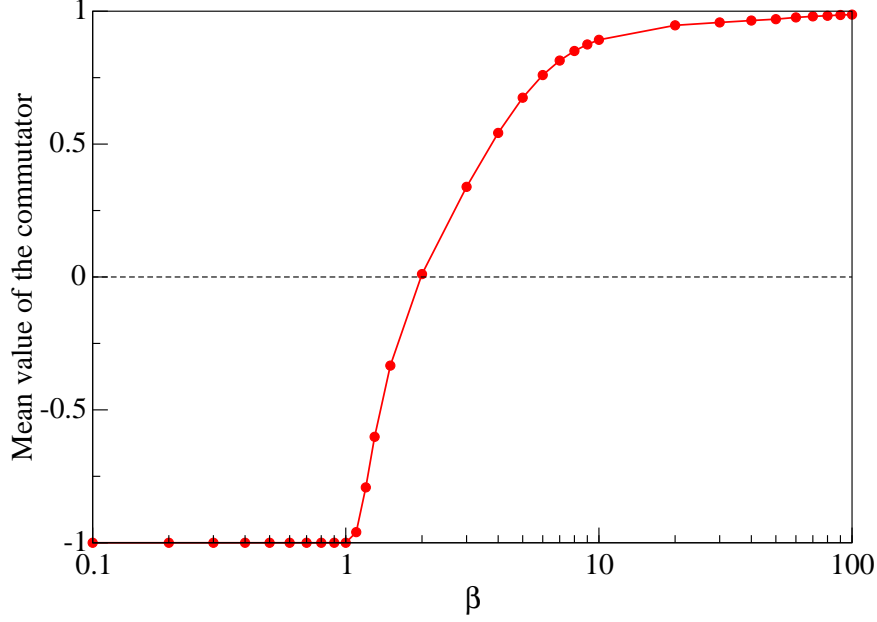


Figure 5.3: Mean value of the variational exciton operators' commutator as a function of the Coulomb interaction strength.

The commutator is:

$$[s_i, s_i^\dagger] = 1 - \sum_{knm} \langle dx_i | n\bar{m} \rangle \langle k\bar{m} | dx_i \rangle e_k^\dagger e_n - \sum_{pnm} \langle dx_i | n\bar{m} \rangle \langle n\bar{p} | dx_i \rangle h_p^\dagger h_{\bar{m}}. \quad (5.13)$$

Again, we calculate the mean value of the commutator, but instead of using the same state $|dx_i\rangle$, the variational procedure allows us to use a state with a mean number of N excitons: $|Ndx_j\rangle$. The latter will be written in the same form as Eq. (5.11) but with coefficients \bar{u}_n and \bar{v}_n . Thus, replacing the explicit form of the states $|dx_i\rangle$ and $|Ndx_j\rangle$, the mean value of the commutator leads to:

$$\langle [s_i, s_i^\dagger] \rangle = 1 - 2 \sum_n v_n^2 \bar{v}_n^2 \prod_{k \neq n} u_k^2. \quad (5.14)$$

The criterion is the same used in Section 3.3, the mean value of the commutator is 1 if the excitons are bosons and is -1 if fermions. We note that the mean value of Eq. (3.7) in a multiexcitonic state like $|Ndx_j\rangle$ is also -1 because there can only be 1 fermion in each state i due to Pauli exclusion principle.

Fig. 5.3 shows the dependence of the mean value of the commutator with the Coulomb interaction β . The basis was composed of 378 single particle harmonic oscillator states, this means that the truncation of the basis was at $n_{max} = 13$. The states $|dx_i\rangle$ and $|Ndx_i\rangle$ used correspond to the ground states of the system with $N_{exc} = 1$ and $N_{exc} = 10$, respectively. We corroborate the results of Section 3.3 where computational issues did not allow us to reach convergence for high values of β . The excitons are fermions in small quantum dots where the harmonic confinement is strong (β small), but are bosons in large QDs where the wavefunctions of charge carriers do not overlap (β big). Also, the transition is sharp when $l_O \sim a_B$, consistently with Ref. [32].

Chapter 6

Bose-Einstein Condensation of Dipolaritons: Finite Temperature Variational Method

Quantum mechanics at zero temperature allows us to describe an isolated system with a ket (wave function) in a Hilbert space. In this situation, we have a complete knowledge of the state of the system, this means that the entropy is zero ($S = 0$), as the third law of thermodynamics states. When the quantum system interacts with a reservoir at a certain temperature, the huge amount of interactions that arise from the thermalization process introduces decoherence to the system and the complete knowledge we had is broken up. In this situation, the system is described by a *density matrix* and the entropy becomes a measurement of the uncertainty we have of the state of the system [41].

The study of quantum systems at finite temperature is of great interest since new phase transitions arise due to the quantum nature of particles. Typical examples of this are the *superconductivity* and *Bose-Einstein condensation*. In Chapters 3 and 5, direct and indirect excitons have been proven to behave like bosons in large QDs then, in the light-matter interacting system, a unitary transformation to dipolariton operators can be performed, in such a way that the operators preserve Bose statistics, i.e., we may expect dipolaritons to condensate. Also, due to the small effective mass excitons and photons have (which leads to a small effective mass for dipolaritons) a higher condensation temperature, compared to the atomic case, is expected for dipolaritons.

In this chapter, the system of two interacting QDs embedded in a microcavity at a finite temperature is modelled. A variational method in a Hartree-Fock-Bogoliubov approximation is developed in order to minimize a proper thermodynamic potential. The effects of the magnetic field in the thermodynamic properties of the system are studied.

6.1 Theory

In analogy with the zero temperature case, the finite temperature treatment starts with a trial statistical density matrix of the form [6, 49]:

$$D = \frac{e^{-\beta K_{ph}}}{Z_{ph}} \prod_{n=1}^{N_{states}} \frac{e^{-\beta K_{eh}^{(n)}}}{Z_{eh}^{(n)}}, \quad (6.1)$$

where $Z_{ph} = \text{Tr} e^{-\beta K_{ph}}$, $Z_{eh}^{(n)} = \text{Tr} e^{-\beta K_{eh}^{(n)}}$ are the partition functions of the photonic and excitonic components, respectively. $K_{ph} = (\hbar\omega - \mu)a^\dagger a$ and $K_{eh}^{(n)}$ is an operator whose form depends on the approximation used, in the Hartree-Fock-Bogoliubov approximation it takes the form:

$$\begin{aligned} K_{eh} = & \frac{1}{2} \sum_n \left(\Delta_{n\bar{n}} e_{n1}^\dagger h_{\bar{n}}^\dagger + \Delta_{n\bar{n}}^* h_{\bar{n}} e_{n1} + \Gamma_{n\bar{n}} e_{n2}^\dagger h_{\bar{n}}^\dagger + \Gamma_{n\bar{n}}^* h_{\bar{n}} e_{n2} + \Omega_{nn} e_{n1}^\dagger e_{n2} + \Omega_{nn}^* e_{n2}^\dagger e_{n1} \right) \\ & - \frac{1}{2} \sum_n \left(\Delta_{n\bar{n}} h_{\bar{n}}^\dagger e_{n1}^\dagger + \Delta_{n\bar{n}}^* e_{n1} h_{\bar{n}} + \Gamma_{n\bar{n}} h_{\bar{n}}^\dagger e_{n2}^\dagger + \Gamma_{n\bar{n}}^* e_{n2} h_{\bar{n}} + \Omega_{nn} e_{n2} e_{n1}^\dagger + \Omega_{nn}^* e_{n1} e_{n2}^\dagger \right) \\ & + \frac{1}{2} \sum_n h_{nn}^{(e1)} \left(e_{n1}^\dagger e_{n1} - e_{n1} e_{n1}^\dagger \right) + \frac{1}{2} \sum_n h_{nn}^{(e2)} \left(e_{n2}^\dagger e_{n2} - e_{n2} e_{n2}^\dagger \right) \\ & + \frac{1}{2} \sum_n h_{nn}^{(h)} \left(h_{\bar{n}}^\dagger h_{\bar{n}} - h_{\bar{n}} h_{\bar{n}}^\dagger \right), \end{aligned}$$

which can be written as:

$$K_{eh} = \frac{1}{2} \sum_n \alpha_n^\dagger \mathcal{H}_{eh}^{(n)} \alpha_n, \quad (6.2)$$

with the definitions:

$$\alpha_n = \begin{pmatrix} e_{n1} \\ e_{n2} \\ h_{\bar{n}} \\ e_{n1}^\dagger \\ e_{n2}^\dagger \\ h_{\bar{n}}^\dagger \end{pmatrix} \quad (6.3)$$

and

$$\mathcal{H}_{eh}^{(n)} = \begin{pmatrix} h_{nn}^{(e1)} & \Omega_{nn} & 0 & 0 & 0 & \Delta_{n\bar{n}} \\ \Omega_{nn}^* & h_{nn}^{(e2)} & 0 & 0 & 0 & \Gamma_{n\bar{n}} \\ 0 & 0 & h_{\bar{n}\bar{n}}^{(h)} & -\Delta_{n\bar{n}} & -\Gamma_{n\bar{n}} & 0 \\ 0 & 0 & -\Delta_{n\bar{n}}^* & -h_{nn}^{(e1)} & -\Omega_{nn}^* & 0 \\ 0 & 0 & -\Gamma_{n\bar{n}}^* & -\Omega_{nn} & -h_{nn}^{(e2)} & 0 \\ \Delta_{n\bar{n}}^* & \Gamma_{n\bar{n}}^* & 0 & 0 & 0 & -h_{\bar{n}\bar{n}}^{(h)} \end{pmatrix}. \quad (6.4)$$

In $\mathcal{H}_{eh}^{(n)}$, the h are single particle energies and $\Delta_{n\bar{n}}$, $\Gamma_{n\bar{n}}$ and Ω_{nn} are gap functions. The matrix $\mathcal{H}_{eh}^{(n)}$ may be interpreted as a quasiparticle hamiltonian in which the complex many-body interactions are simplified as pairing interactions.

As a finite temperature variational method, the idea is to minimize the thermodynamic potential:

$$\phi(D) = \bar{E} - \mu \bar{N}_{dip} - \frac{1}{\beta_T} S, \quad (6.5)$$

where we have defined $\bar{E} = \text{Tr}[DH]$, $\bar{N}_{dip} = \text{Tr}[DN_{dip}]$, $S = -\text{Tr}[D \ln D]$ and $\beta_T = 1/k_B T$. When minimizing the potential (6.5) a conserved number of particles is assumed, since dipolaritons recombine, this assumption is valid only if their lifetime is longer than the time required to reach thermal equilibrium. From the indirect exciton component, we may expect dipolaritons to have lifetimes on the order of microseconds [22], time enough for the system to reach thermal equilibrium. Introducing the generalized density matrix (not to be confused with the statistical density matrix D):

$$R_{eh}^{(n)} = \begin{pmatrix} \rho_{nn}^{(e1)} & \tau_{nn} & 0 & 0 & 0 & \kappa_{n\bar{n}}^{(1)} \\ \tau_{nn}^* & \rho_{nn}^{(e2)} & 0 & 0 & 0 & \kappa_{n\bar{n}}^{(2)} \\ 0 & 0 & \rho_{\bar{n}\bar{n}}^{(h)} & -\kappa_{n\bar{n}}^{(1)} & -\kappa_{n\bar{n}}^{(2)} & 0 \\ 0 & 0 & -\kappa_{n\bar{n}}^{(1)*} & 1 - \rho_{nn}^{(e1)} & -\tau_{nn}^* & 0 \\ 0 & 0 & -\kappa_{n\bar{n}}^{(2)*} & -\tau_{nn} & 1 - \rho_{nn}^{(e2)} & 0 \\ \kappa_{n\bar{n}}^{(1)*} & \kappa_{n\bar{n}}^{(2)*} & 0 & 0 & 0 & 1 - \rho_{\bar{n}\bar{n}}^{(h)} \end{pmatrix}, \quad (6.6)$$

the minimization procedure $\delta\phi = 0$ leads to the following conditions:

$$\frac{\partial(\bar{E} - \mu\bar{N}_{dip})}{\partial\sigma} = 0, \quad \frac{\partial(\bar{E} - \mu\bar{N}_{dip})}{\partial(R_{eh}^{(n)})^{ij}} = \frac{1}{2} (\mathcal{H}_{eh}^{(n)})^{ij}. \quad (6.7)$$

In Eq. (6.6) we have defined the single-particle density matrices $\rho_{nn}^{(ei)} = \text{Tr}[De_{ni}^\dagger e_{ni}]$ and $\rho_{\bar{n}\bar{n}}^{(h)} = \text{Tr}[Dh_{\bar{n}}^\dagger h_{\bar{n}}]$, and the pair matrices $\kappa_{n\bar{n}}^{(i)} = \text{Tr}[Dh_{\bar{n}} e_{ni}]$ and $\tau_{nn} = \text{Tr}[De_{n2}^\dagger e_{n1}]$. The mean value \bar{E} is calculated with the help of Wick's theorem [40] and a Lagrange multiplier λ is introduced to take into account the charge conservation constrain. The explicit form of the equations that arise from the minimization of ϕ , Eq. (6.7), are the single particle energies:

$$h_{nn}^{(e1)} = t_{nn}^{(e1)} + \beta \sum_{k \neq n} (\langle kn|V(0)|kn\rangle - \langle kn|V(0)|nk\rangle) \rho_{kk}^{(e1)} - \beta \sum_{k \neq n} \langle kn|V(0)|kn\rangle \rho_{\bar{k}\bar{k}}^{(h)} - \beta \langle nn|V(0)|nn\rangle + \gamma \sum_{k \neq n} \langle kn|V(a)|kn\rangle \rho_{kk}^{(e2)} - \frac{\mu}{2} - \lambda, \quad (6.8)$$

$$h_{nn}^{(e2)} = t_{nn}^{(e2)} + \beta \sum_{k \neq n} (\langle kn|V(0)|kn\rangle - \langle kn|V(0)|nk\rangle) \rho_{kk}^{(e2)} - \gamma \sum_{k \neq n} \langle kn|V(a)|kn\rangle \rho_{\bar{k}\bar{k}}^{(h)} - \gamma \langle nn|V(a)|nn\rangle + \gamma \sum_{k \neq n} \langle kn|V(a)|kn\rangle \rho_{kk}^{(e1)} - \frac{\mu}{2} - \lambda, \quad (6.9)$$

$$\begin{aligned}
h_{\bar{n}\bar{n}}^{(h)} &= t_{\bar{n}\bar{n}}^{(h)} + \beta \sum_{k \neq n} (\langle kn|V(0)|kn\rangle - \langle kn|V(0)|nk\rangle) \rho_{\bar{k}\bar{k}}^{(h)} - \beta \sum_{k \neq n} \langle kn|V(0)|kn\rangle \rho_{kk}^{(e1)} \\
&\quad - \gamma \sum_{k \neq n} \langle kn|V(a)|kn\rangle \rho_{kk}^{(e2)} - \frac{\mu}{2} + \lambda,
\end{aligned} \tag{6.10}$$

the generalized gap equations:

$$\Delta_{n\bar{n}} = g\sigma^* - \beta \sum_{k \neq n} \langle kn|V(0)|nk\rangle \kappa_{n\bar{n}}^{(1)*}, \tag{6.11}$$

$$\Omega_{nn} = T_e - \gamma \sum_{k \neq n} \langle kn|V(a)|nk\rangle \tau_{kk}^*, \tag{6.12}$$

$$\Gamma_{n\bar{n}} = -\gamma \sum_{k \neq n} \langle kn|V(a)|nk\rangle \kappa_{n\bar{n}}^{(2)*}, \tag{6.13}$$

and the constrains:

$$0 = (\hbar\omega - \mu)\sigma + g \sum_n \kappa_{n\bar{n}}^{(1)}, \tag{6.14}$$

$$\bar{N}_{dip} = |\sigma|^2 + \frac{1}{e^{\beta_T(\hbar\omega - \mu)} - 1} + \frac{1}{2} \sum_n \left(\rho_{nn}^{(e1)} + \rho_{nn}^{(e2)} + \rho_{\bar{n}\bar{n}}^{(h)} \right), \tag{6.15}$$

$$\sum_n \left(\rho_{nn}^{(e1)} + \rho_{nn}^{(e2)} - \rho_{\bar{n}\bar{n}}^{(h)} \right) = 0. \tag{6.16}$$

The rest of the equations necessary to obtain a closed set are obtained from the eigenvalue problem [6]:

$$\mathcal{H}_{eh}^{(n)} X_n = E_n X_n. \tag{6.17}$$

There are three positive eigenvalues $E_n^{(1,2,3)}$ associated to three eigenvectors $V_n^{(1,2,3)}$. The other three eigenvalues correspond to $-E_n^{(1,2,3)}$ and are associated to the eigenvectors $W_n^{(1,2,3)}$. With the eigensystem the generalized density matrix is constructed as:

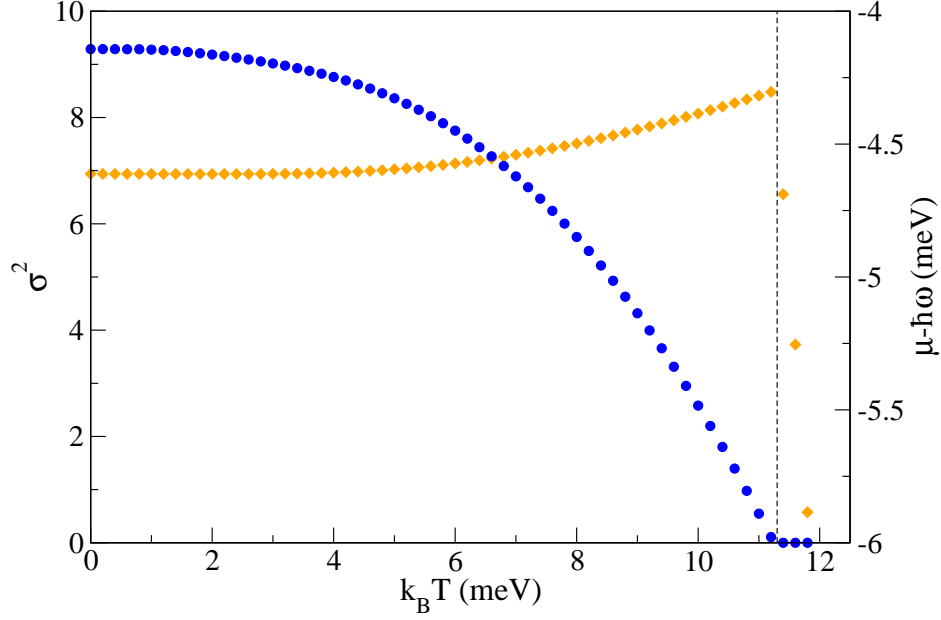


Figure 6.1: Temperature dependence of the number of photons in the condensate (circles) and the chemical potential (diamonds). The dashed line at $k_B T = 11.2 \text{ meV}$ marks the critical temperature. $B = 9T$, $N_{dip} = 10$.

$$R_{eh}^{(n)} = \sum_{i=1}^3 \left(\frac{V_n^{(i)} V_n^{(i)\dagger}}{e^{\beta T E_n^{(i)}} + 1} + \frac{W_n^{(i)} W_n^{(i)\dagger}}{e^{-\beta T E_n^{(i)}} + 1} \right), \quad (6.18)$$

from which we obtain the single-particle density matrices $\rho_{nn}^{(e1)}$, $\rho_{nn}^{(e2)}$, $\rho_{\bar{n}\bar{n}}^{(h)}$ and the pair matrices $\kappa_{n\bar{n}}^{(1)}$, $\kappa_{n\bar{n}}^{(2)}$ and τ_{nn} . Eqs. (6.8)-(6.18) are to be iteratively solved until two successive iterations yield the same generalized density matrix R_{eh} , chemical potential μ and mean number of photons in the condensate $|\sigma|^2$, to the desired accuracy [6].

6.2 Bose-Einstein condensation of dipolaritons

We iteratively solved the equations from the previous section using 3 Landau levels with 120 states each (a total of 360 single-particle states), the parameters used where: $\hbar\omega_h = 2 \text{ meV}$,

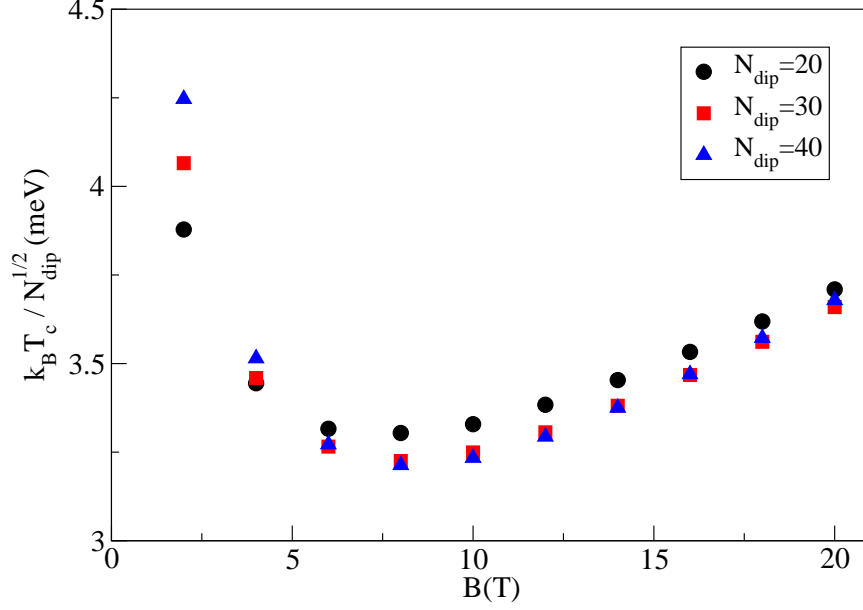


Figure 6.2: Scaling of the critical temperature vs magnetic field.

$\hbar\omega_{e1} = 3\text{meV}$, $\hbar\omega_{e2} = 4\text{meV}$, $\hbar\omega = 860\text{meV}$, $E_0^h = 13\text{meV}$, $E_0^{e1} = 18\text{meV}$, $a = 15\text{nm}$ and $T_e = 2\text{meV}$. Fig. 6.1 shows the temperature dependence of the number of photons in the condensate $|\sigma|^2$ and the chemical potential for a system of 10 dipolaritons. We identify the phase transition at $k_B T \approx 11.2\text{meV}$ as Bose-Einstein condensation of dipolaritons [6, 49]. This energy corresponds to $T \approx 130\text{K}$, so that the high condensation temperature of bosons in solid state systems is demonstrated. It is important to clarify that the photon number is given by:

$$N_{ph} = |\sigma|^2 + \frac{1}{e^{\beta_T(\hbar\omega - \mu)} - 1}, \quad (6.19)$$

where $|\sigma|^2$ is the number of particles in the condensate and the other term corresponds to particles that are excited out of the condensate as a result of thermal fluctuations of the phonons [6].

Fig. 6.2 displays the effect of the magnetic field on the critical temperature for condensation T_c , there, we see that the field can be used to tune the condensation temperature of dipolaritons; the range of tuning increases with the number of particles. In the same figure the scaling of the critical temperature with the size of the system is shown to behave as $T_c \sim N_{dip}^{1/2}$.

Chapter 7

Conclusions

In this thesis we have investigated the properties of a Quantum Dot Molecule embedded in a microcavity from the point of view of dipolaritons. A finite system hamiltonian of electrons and holes confined in a harmonic potential, under the presence of a magnetic field, was proposed to model the system. Three theoretical methods were used to deal with the hamiltonian: an exact diagonalization was performed to study single-particle properties of direct excitons, indirect excitons and dipolaritons; a variational approach at zero temperature was developed to study the many-body properties; and a variational method in a Hartree-Fock-Bogoliubov approximation was used to find the Bose-Einstein condensation of dipolaritons. The main results of this work are the following:

- The energies of direct and indirect excitons can be tuned by means of the magnetic field.
- The statistical properties of excitons depend on the size of the QDs. Both fermionic and bosonic regimes are reachable.
- Indirect excitons are of great impact on system's properties, their extra tuning with a bias voltage provides an extra control channel.
- Our finite system model successfully reproduces the expected avoided crossings between dipolariton branches and provides extra information not obtainable from effective models.

- The magnetic field can be used to control: the energy and composition of dipolaritons, the intensity and energy of emission, the production of photons in the microcavity, and the magnetic response of the system (from paramagnetic to diamagnetic).
- Dipolaritons in QDs are able to condensate, moreover, the critical temperature can be increased with the magnetic field.

7.1 Future Work

The theory developed in this thesis can be extended in several directions. Some interesting future works can be to:

- Study the effects of the tunnelling rates in the statistics of excitons and dipolaritons.
- Introduce dissipation channels as are: spontaneous emission, photon leakage through cavity mirrors and pumping.
- Use the exact diagonalization to investigate biexcitons.
- Quantitatively discuss the validity of effective models compared to this finite system one.
- Study the entanglement in the system.

Appendix A

Coulomb Matrix Elements

This chapter is dedicated to the explicit calculation of the matrix elements of the Coulomb interaction between single particle states. The method described here is the one developed by Ref. [35] and [40]. We consider two particles in parallel layers separated by a vertical vector \vec{a} , each particle is represented by a 2D coordinate vector \vec{r}_1 and \vec{r}_2 as shown in Fig. A.1. The integral to calculate is:

$$\langle ij|V(a)|kl\rangle = \int \frac{d^2r_1 d^2r_2}{|\vec{r}_1 - \vec{r}_2 + \vec{a}|} \phi_i^*(\vec{r}_1) \phi_j^*(\vec{r}_2) \phi_k(\vec{r}_1) \phi_l(\vec{r}_2), \quad (\text{A.1})$$

where the wave functions $\phi_i(\vec{r})$ associated to the state $|i\rangle = |n_i, l_i\rangle$ are:

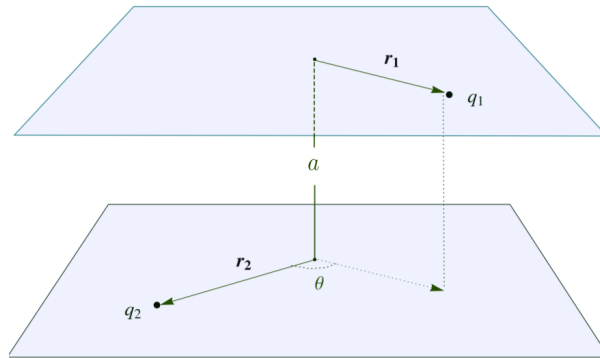


Figure A.1: Bilayer of interplane distance a , with charge carriers at \vec{r}_1 and \vec{r}_2 , and relative angle θ . Image edited from Ref. [35].

$$\phi_i(\vec{r}) = \phi_{(n_i, l_i)}(\vec{r}) = C_{n_i, |l_i|} r^{|l_i|} L_{n_i}^{|l_i|}(r^2) e^{-r^2/2} e^{i l_i \theta}, \quad (\text{A.2})$$

with $C_{n_i, |l_i|} = \sqrt{n_i! / [\pi(n_i + |l_i|)!]}$ a normalization constant, $L_n^l(x)$ the associated Laguerre polynomial and $d^2r = r dr d\theta$.

A.1 Solving the integral

The explicit form of Eq. (A.1) is:

$$\begin{aligned} \langle ij|V(a)|kl\rangle &= C_{n_i, |l_i|} C_{n_j, |l_j|} C_{n_k, |l_k|} C_{n_l, |l_l|} \int \frac{d^2r_1 d^2r_2}{|\vec{r}_1 - \vec{r}_2 + \vec{a}|} r_1^{|l_i|+|l_k|} r_2^{|l_j|+|l_l|} \\ &\times L_{n_i}^{|l_i|}(r_1^2) L_{n_k}^{|l_k|}(r_1^2) L_{n_j}^{|l_j|}(r_2^2) L_{n_l}^{|l_l|}(r_2^2) e^{-(r_1^2+r_2^2)} e^{i(l_k-l_i)\theta_1 + i(l_l-l_j)\theta_2}. \end{aligned} \quad (\text{A.3})$$

Using the transformation $\theta = \theta_1 - \theta_2$ and $\Theta = (\theta_1 + \theta_2)/2$, we obtain an angular momentum conservation from the integral in Θ :

$$\int_0^{2\pi} d\Theta e^{i(l_k-l_i+l_l-l_j)\Theta} = 2\pi \delta_{l_i+l_j, l_k+l_l}. \quad (\text{A.4})$$

Now, using the relation $1/\sqrt{x} = 1/\sqrt{\pi} \int_0^\infty (dt/t^{1/2}) e^{-tx}$, we expand the denominator:

$$\begin{aligned} \frac{1}{|\vec{r}_1 - \vec{r}_2 + \vec{a}|} &= \frac{1}{\sqrt{r_1^2 + r_2^2 + a^2 - 2r_1 r_2 \cos \theta}} \\ &= \frac{1}{\sqrt{\pi}} \int_0^\infty \frac{dt}{t^{1/2}} e^{-t(r_1^2+r_2^2+a^2-2r_1 r_2 \cos \theta)} \\ &= \frac{1}{\sqrt{\pi}} \int_0^\infty \frac{dt}{t^{1/2}} e^{-t(r_1^2+r_2^2+a^2)} \sum_{n=0}^\infty \frac{2^n t^n r_1^n r_2^n \cos^n \theta}{n!}, \end{aligned}$$

in the last step we expanded the exponential in Taylor series. With the above, the integral with respect to the angle θ , taking into account the angular momentum conservation, is:

$$\begin{aligned}
I_\theta &= \int_0^{2\pi} d\theta e^{\frac{i}{2}(l_k - l_i + l_j - l_l)\theta} \cos^n \theta \\
&= \begin{cases} \frac{2\pi n!}{2^n \left(\frac{n-|l_k-l_i|}{2}\right)! \left(\frac{n+|l_k-l_i|}{2}\right)!}, & \text{for } n - |l_k - l_i| \text{ even} \\ 0, & \text{otherwise} \end{cases}. \tag{A.5}
\end{aligned}$$

The Coulomb's element from Eq. (A.3), defining $p = (n - |l_k - l_i|)/2$, is then:

$$\begin{aligned}
\langle ij|V(a)|kl\rangle &= 4\pi^{3/2} \delta_{l_i+l_j, l_k+l_l} C_{n_i, |l_i|} C_{n_j, |l_j|} C_{n_k, |l_k|} C_{n_l, |l_l|} \\
&\times \int_0^\infty dr_1 \int_0^\infty dr_2 \int_0^\infty \frac{dt}{t^{1/2}} e^{-t(r_1^2+r_2^2+a^2)} \sum_{p=0}^\infty \frac{t^{2p+|l_k-l_i|}}{p!(p+|l_k-l_i|)!} \\
&\times r_1^{1+2p+|l_i|+|l_k|-l_i} r_2^{1+2p+|l_j|+|l_l|+|l_k-l_i|} \\
&\times L_{n_i}^{|l_i|}(r_1^2) L_{n_k}^{|l_k|}(r_1^2) L_{n_j}^{|l_j|}(r_2^2) L_{n_l}^{|l_l|}(r_2^2) e^{-(r_1^2+r_2^2)}. \tag{A.6}
\end{aligned}$$

Using the transformations $x_1 = r_1^2$ and $x_2 = r_2^2$ and the closed form of the associated Laguerre polynomials:

$$L_n^l(x) = \sum_{m=0}^n (-1)^m \frac{\Gamma(n+l+1)}{\Gamma(m+l+1)\Gamma(n-m+1)\Gamma(m+1)} x^m := \sum_{m=0}^n G(n, l, m) x^m, \tag{A.7}$$

we obtain:

$$\begin{aligned}
\langle ij|V(a)|kl\rangle &= \pi^{3/2} \delta_{l_i+l_j, l_k+l_l} C_{n_i, |l_i|} C_{n_j, |l_j|} C_{n_k, |l_k|} C_{n_l, |l_l|} \sum_{p=0}^\infty \frac{1}{p!(p+|l_k-l_i|)!} \\
&\times \sum_{m_i=0}^{n_i} G(n_i, |l_i|, m_i) \sum_{m_k=0}^{n_k} G(n_k, |l_k|, m_k) \sum_{m_j=0}^{n_j} G(n_j, |l_j|, m_j) \sum_{m_l=0}^{n_l} G(n_l, |l_l|, m_l) \\
&\times \int_0^\infty dt e^{-ta^2} t^{2p+|l_k-l_i|-1/2} \int_0^\infty dx_1 x_1^{\frac{1}{2}(2p+2m_i+2m_k+|l_i|+|l_k|+|l_k-l_i|)} e^{-x_1(1+t)} \\
&\times \int_0^\infty dx_2 x_2^{\frac{1}{2}(2p+2m_j+2m_l+|l_j|+|l_l|+|l_l-l_j|)} e^{-x_2(1+t)}.
\end{aligned}$$

The integrals in x_1 and x_2 have the following solutions:

$$I_{x_1} = (1+t)^{-(1+p+m_i+m_k+l_{ik})}\Gamma[1+p+m_i+m_k+l_{ik}] \quad (\text{A.8})$$

$$I_{x_2} = (1+t)^{-(1+p+m_j+m_l+l_{jl})}\Gamma[1+p+m_j+m_l+l_{jl}], \quad (\text{A.9})$$

where we have defined $l_{ik} = (|l_i| + |l_k| + |l_k - l_i|)/2$ and similarly for l_{jl} for the sake of simplifying the notation. At this point, we only have pendant the integral in t :

$$\begin{aligned} \langle ij|V(a)|kl\rangle &= \pi^{3/2}\delta_{l_i+l_j,l_k+l_l}C_{n_i,|l_i|}C_{n_j,|l_j|}C_{n_k,|l_k|}C_{n_l,|l_l|}\sum_{p=0}^{\infty}\frac{1}{p!(p+|l_k-l_i|)!} \\ &\times \sum_{m_i=0}^{n_i}G(n_i,|l_i|,m_i)\sum_{m_k=0}^{n_k}G(n_k,|l_k|,m_k)\sum_{m_j=0}^{n_j}G(n_j,|l_j|,m_j) \\ &\times \sum_{m_l=0}^{n_l}G(n_l,|l_l|,m_l)\Gamma[1+p+m_i+m_k+l_{ik}]\Gamma[1+p+m_j+m_l+l_{jl}] \\ &\times \int_0^{\infty}dt e^{-ta^2}t^{2p+|l_k-l_i|-1/2}(1+t)^{-(2+2p+m_i+m_k+m_j+m_l+l_{ik}+l_{jl})}. \end{aligned}$$

To evaluate this last integral we make use of the following result:

$$\int_0^{\infty}dte^{-\alpha t}t^{\beta}(1+t)^{-\gamma} = \Gamma(\beta+1)U(1+\beta;2+\beta+\gamma;\alpha), \text{ if } \Re \beta > -1 \text{ and } \Re \alpha > 0. \quad (\text{A.10})$$

The integral we need to solve meets the requirements, so the solution is expressed in terms of $U(a; b; z)$, the confluent hypergeometric function of the second kind, which is related to the confluent hypergeometric function of the first kind ${}_1F_1(a; b; z)$ by:

$$U(a; b; z) = \pi \csc(\pi b) \left[\frac{{}_1F_1(a; b; z)}{\Gamma(a-b+1)\Gamma(b)} - \frac{z^{1-b}{}_1F_1(a-b+1; 2-b; z)}{\Gamma(a)\Gamma(2-b)} \right] \quad (\text{A.11})$$

Coulomb's element is finally expressed as:

$$\begin{aligned}
\langle ij|V(a)|kl\rangle &= \pi^{3/2}\delta_{l_i+l_j,l_k+l_l}C_{ijkl}\sum_{p=0}^{\infty}\frac{1}{p!(p+|l_k-l_i|)!}\sum_{m_i=0}^{n_i}\sum_{m_k=0}^{n_k}\sum_{m_j=0}^{n_j}\sum_{m_l=0}^{n_l}G_{ijkl} \\
&\times \Gamma[1+p+\alpha_{ik}]\Gamma[1+p+\alpha_{jl}]\left\{\frac{\Gamma(\nu_{ik})\Gamma(\eta_{ijkl})}{\Gamma(\nu_{ik}+\eta_{ijkl})}{}_1F_1(\nu_{ik};1-\eta_{ijkl};a^2)\right. \\
&\quad \left.+a^{2\eta_{ijkl}}\Gamma(-\eta_{ijkl}){}_1F_1(\nu_{ik}+\eta_{ijkl};1+\eta_{ijkl};a^2)\right\}, \quad (\text{A.12})
\end{aligned}$$

where we have employed the following definitions to simplify the notation: $C_{ijkl} = \prod_{x=i,j,k,l} C_{n_x,|l_x|}$, $G_{ijkl} = \prod_{x=i,j,k,l} G(n_x, |l_x|, m_x)$, $\alpha_{ik} = m_i + m_k + l_{ik}$, $\nu_{ik} = 2p + |l_k - l_i| + 1/2$ and $\eta_{ijkl} = 3/2 - |l_k - l_i| + m_i + m_j + m_k + m_l + l_{ik} + l_{jl}$.

It is important to notice that the procedure has been developed for charge carriers in different planes separated by an arbitrary distance a . The situation of charge carriers in the same plane (in the same QD) is reproduced by Eq. (A.12) evaluating at $a = 0$.

We have been able to express the Coulomb interaction term as a single infinite series (variable p) in Eq. (A.12). Computationally, the infinite series must be truncated until the element converges to the desired accuracy, however, it is still infeasible if we want to calculate a huge number of elements. An algorithm to accelerate the convergence of the series has to be employed.

A.2 Series acceleration

As in Ref. [35] we use the u-type Levin transform as the series acceleration algorithm. Let us start with the series:

$$s = \sum_{n=0}^{\infty} a_n. \quad (\text{A.13})$$

The u-type Levin transform reduces the problem of calculating the series to a $k + 1$ -dimensional matrix inversion one. If σ is an approximation of the exact value s of the series and σ_m the m -th partial sum, we have the following set of equations:

$$\sigma_m = \sigma + \omega_m \sum_{i=0}^{k-1} C_i \psi_i(m), \quad (\text{A.14})$$

with m running from a chosen m_0 to $m_0 + k$. The functions $\psi_i(m)$ satisfy three conditions: first, $\psi_0(m) = 1 \forall m$; second, for $i > 0$ the functions satisfy $\psi_i(m) \rightarrow 0$ when $m \rightarrow \infty$; and third, $\psi_{i+1}(m) = \mathcal{O}(\psi_i(m))$, so that when taking the limit $m \rightarrow \infty$, all the $i \neq 0$ terms vanish at the same rate. We, now, have a system of $k + 1$ equations to solve for the $k + 1$ unknowns: σ and $\{C_i\}$. The u-type Levin transform uses the choices $\psi_i(m) = (m + \beta)^{-i}$ and $\omega_m = ma_m$, which have proven to behave well for a large family of series [16]. β is a real parameter to be chosen and that might help to improve the rate of convergence. The bigger k the better the approximation.

Bibliography

- [1] InGaAs - Indium Gallium Arsenide: Band structure and carrier concentration, <http://www.ioffe.ru/SVA/NSM/Semicond/GaInAs/bandstr.html>. [Online; accessed 8-November-2015].
- [2] InGaAs - Indium Gallium Arsenide: Optical properties, <http://www.ioffe.ru/SVA/NSM/Semicond/GaInAs/optic.html>. [Online; accessed 9-November-2015].
- [3] A. Babiński, J. Borysiuk, S. Kret, M. Czyż, A. Golnik, S. Raymond, and Z. R. Wasilewski. Natural quantum dots in the InAsGaAs wetting layer. *Applied Physics Letters*, 92(17), 2008.
- [4] R. Balili, V. Hartwell, D. Snoke, L. Pfeiffer, and K. West. Bose-Einstein Condensation of Microcavity Polaritons in a Trap. *Science*, 316(5827):1007–1010, 2007.
- [5] G. Bastard. *Wave mechanics applied to semiconductor heterostructures*. Lés editions de physique, 1992.
- [6] J.P. Blaizot and G. Ripka. *Quantum theory of finite systems*. MIT Press Ltd., 1986.
- [7] L.V. Butov. Exciton condensation in coupled quantum wells. *Solid State Communications*, 127(2):89–98, 2003.
- [8] L.V. Butov. Condensation and pattern formation in cold exciton gases in coupled quantum wells. *Journal of Physics: Condensed Matter*, 16(50):R1577, 2004.
- [9] T. Byrnes, N. Y. Kim, and Y. Yamamoto. Excitonpolariton condensates. *Nature Physics*, 10(11):803–813, 2014.
- [10] T. Byrnes, G.V. Kolmakov, R.Y. Kezerashvili, and Y. Yamamoto. Effective interaction and condensation of dipolaritons in coupled quantum wells. *Phys. Rev. B*, 90:125314, Sep 2014.
- [11] M. Combescot and O. Betbeder-Matibet. The effective bosonic hamiltonian for excitons reconsidered. *EPL (Europhysics Letters)*, 58(1):87, 2002.
- [12] M. Combescot and C. Tanguy. New criteria for bosonic behavior of excitons. *EPL (Europhysics Letters)*, 55(3):390, 2001.

- [13] P. Cristofolini, G. Christmann, S.I. Tsintzos, G. Deligeorgis, G. Konstantinidis, Z. Hatzopoulos, P.G. Savvidis, and J.J. Baumberg. Coupling quantum tunneling with cavity photons. *Science*, 336(6082):704–707, 2012.
- [14] P.R. Eastham and P.B. Littlewood. Bose condensation of cavity polaritons beyond the linear regime: The thermal equilibrium of a model microcavity. *Phys. Rev. B*, 64:235101, Nov 2001.
- [15] L.D. Faddeev and S.P. Merkuriev. *Quantum Scattering Theory for Several Particle Systems*. Springer Netherlands, 1993.
- [16] T. Fessler, W.F. Ford, and D.A. Smith. Hurry: An acceleration algorithm for scalar sequences and series. *ACM Trans. Math. Softw.*, 9(3):346–354, September 1983.
- [17] A.L. Fetter and J.D. Walecka. *Quantum Theory of Many-particle Systems*. Dover Books on Physics. Dover Publications, 2003.
- [18] A. Gärtner, A.W. Holleitner, J.P. Kotthaus, and D. Schuh. Drift mobility of long-living excitons in coupled GaAs quantum wells. *Applied Physics Letters*, 89(5):052108, 2006.
- [19] C. Gerry and P. Knight. *Introductory Quantum Optics*. Cambridge University Press, 2005.
- [20] A.V. Gorbunov, A.V. Larionov, and V.B. Timofeev. Luminescence kinetics of dipolar excitons in circular traps. *JETP Letters*, 86(1):46–50, 2007.
- [21] A.V. Gorbunov and V.B. Timofeev. Dipolar excitons indirect in real and momentum space in a GaAs/AlAs heterostructure. *Semiconductors*, 49(1):44–49, 2015.
- [22] F. Grasselli, A. Bertoni, and G. Goldoni. Space- and time-dependent quantum dynamics of spatially indirect excitons in semiconductor heterostructures. *The Journal of Chemical Physics*, 034701, 2015.
- [23] H. Haug and S.W. Koch. *Quantum Theory of the Optical and Electronic Properties of Semiconductors*. Allied Publishers, 2004.
- [24] L. Jacak, A. Wojs, and P. Hawrylak. *Quantum Dots*. Springer Berlin Heidelberg, 1998.
- [25] M.S. Jun, D.Y. Jeong, S.H. Lee, K. Heo, J.E. Oh, S.W. Hwang, and D. Ahn. Transport experiments on inas self-assembled quantum dots in the microwave regime. *Phys. Rev. B*, 72:085319, Aug 2005.
- [26] A. Kavokin, J.J. Baumberg, G. Malpuech, and F.P. Laussy. *Microcavities*. Oxford science publications. OUP Oxford, 2011.
- [27] K. Kristinsson, O. Kyriienko, T.C.H. Liew, and I.A. Shelykh. Continuous terahertz emission from dipolaritons. *Phys. Rev. B*, 88:245303, Dec 2013.

- [28] K. Kristinsson, O. Kyriienko, and I.A. Shelykh. Terahertz laser based on dipolaritons. *Physical Review A - Atomic, Molecular, and Optical Physics*, 89(2):1–8, 2014.
- [29] O. Kyriienko, A.V. Kavokin, and I.A. Shelykh. Superradiant terahertz emission by dipolaritons. *Phys. Rev. Lett.*, 111:176401, Oct 2013.
- [30] O. Kyriienko, I.A. Shelykh, and T.C.H. Liew. Tunable single-photon emission from dipolaritons. *Physical Review A*, 90(3):033807, September 2014.
- [31] F.P. Laussy, E. del Valle, and C. Tejedor. Luminescence spectra of quantum dots in microcavities. I. Bosons. *Phys. Rev. B*, 79(23):235325, June 2009.
- [32] F.P. Laussy, M.M. Glazov, A. Kavokin, D.M. Whittaker, and G. Malpuech. Statistics of excitons in quantum dots and their effect on the optical emission spectra of microcavities. *Phys. Rev. B*, 73:115343, Mar 2006.
- [33] I.V. Lerner and Y.E. Lozovik. Two-dimensional electron-hole system in a strong magnetic field as an almost ideal exciton gas. *Zh. Eksp. Teor. Fiz.*, 80:763–770, 1981.
- [34] R.D. Mattuck. *A Guide to Feynman Diagrams in the Many-body Problem*. Dover Books on Physics Series. Dover Publications, 1976.
- [35] I. Mondragon-Shem, B.A. Rodríguez, and F.E. López. Efficient calculation of Coulomb matrix elements for bilayers of confined charge carriers with arbitrary spatial separation. *Computer Physics Communications*, 181(9):1510–1516, 2010.
- [36] K. Müller, A. Bechtold, C. Ruppert, M. Zecherle, G. Reithmaier, M. Bichler, H.J. Krenner, G. Abstreiter, A.W. Holleitner, J.M. Villas-Boas, M. Betz, and J.J. Finley. Electrical control of interdot electron tunneling in a double InGaAs quantum-dot nanostructure. *Phys. Rev. Lett.*, 108:197402, May 2012.
- [37] E.U. Rafailov. *The Physics and Engineering of Compact Quantum Dot-based Lasers for Biophotonics*. Wiley, 2013.
- [38] B.J. Riel. An introduction to self-assembled quantum dots. *American Journal of Physics*, 76(8):750–757, 2008.
- [39] B.A. Rodriguez, A. Gonzalez, L. Quiroga, F.J. Rodriguez, and R. Capote. Crossover between the electron-hole phase and the BCS excitonic phase in quantum dots. *International Journal of Modern Physics B*, 14(01):71–83, 2000.
- [40] B.A. Rodríguez Rey. *Núcleos Artificiales*. PhD thesis, Universidad de Antioquia, 2002, unpublished.
- [41] J.P. Sethna. *Statistical mechanics: Entropy, order parameters, and complexity*. Clarendon Press - Oxford University Press, 2011.
- [42] A.G. Silva, F.E. Lopez, P.S.S. Guimares, M.P. Pires, P.L. Souza, S.M. Landi, J.M. Villas-Bas, G.S. Vieira, H. Vinck-Posada, and B.A. Rodriguez. Tunneling through

- stacked inas/ingaas/inp self-assembled quantum dots in a magnetic field. *Journal of Applied Physics*, 110(8):-, 2011.
- [43] J. Smoliner, W. Demmerle, F. Hirler, E. Gornik, G. Weimann, M. Hauser, and W. Schlapp. Tunneling processes between Landau levels and quantum-wire states. *Phys. Rev. B*, 43:7358–7361, Mar 1991.
- [44] M.H. Son, J.H. Oh, D.Y. Jeong, D. Ahn, M.S. Jun, S.W. Hwang, J.E. Oh, and L.W. Engel. Magnetotransport measurements through stacked inas self-assembled quantum dots. *Applied Physics Letters*, 82(8), 2003.
- [45] S. Tarucha, T. Fujisawa, K. Ono, D.G. Austing, T.H. Oosterkamp, W.G. van der Wiel, and L.P. Kouwenhoven. Elastic and inelastic single electron tunneling in coupled two dot system. *Microelectronic Engineering*, 47(14):101 – 105, 1999. New Phenomena in Mesoscopic Structures.
- [46] C.A. Vera, H. Vinck-Posada, and A. González. Polariton lasing in a multilevel quantum dot strongly coupled to a single photon mode. *Phys. Rev. B*, 80:125302, Sep 2009.
- [47] H. Vinck, B.A. Rodriguez, and A. Gonzalez. A multiexcitonic quantum dot in an optical microcavity. *Physica E: Low-dimensional Systems and Nanostructures*, 35(1):99 – 102, 2006.
- [48] H. Vinck-Posada, B.A. Rodriguez, and A. Gonzalez. Mean-field dynamics of a quantum dot-microcavity system. *Physica E: Low-dimensional Systems and Nanostructures*, 27(4):427 – 438, 2005.
- [49] H. Vinck-Posada, B.A. Rodriguez, and A. Gonzalez. Micropillar resonator in a magnetic field: Zero and finite temperature cases. *Superlattices and Microstructures*, 43(56):500 – 506, 2008.
- [50] H. Vinck-Posada, B.A. Rodriguez, P.S.S. Guimaraes, A. Cabo, and A. Gonzalez. Photon emission as a source of coherent behavior of polaritons. *Phys. Rev. Lett.*, 98:167405, Apr 2007.
- [51] A. Wojs, P. Hawrylak, S. Fafard, and L. Jacak. Electronic structure and magneto-optics of self-assembled quantum dots. *Phys. Rev. B*, 54:5604–5608, Aug 1996.